European Journal of Mechanics B/Fluids ▮ (▮▮▮▮) ▮▮▮–▮▮▮

Contents lists available at ScienceDirect

European Journal of Mechanics B/Fluids

journal homepage: www.elsevier.com/locate/ejmflu

Combined effects of magnetic field and rheological properties on the peristaltic flow of a compressible fluid in a microfluidic channel

Sara I. Abdelsalam [a,b,*], Kambiz Vafai [a]

[a] Department of Mechanical Engineering, University of California, Riverside, CA 92521, USA

[b] Basic Science Department, Faculty of Engineering, The British University in Egypt, Al-Shorouk City, Cairo 11837, Egypt

HIGHLIGHTS

- MHD peristaltic flow of compressible Jeffrey fluid is modeled in a microchannel.
- Combined effects of magnetic field and viscoelastic fluid are discussed.
- Increasing the magnetic parameter makes the fluid less prone to nonlinear effects.
- Flow becomes slow due to the suppression effect of the retardation time.
- Quadratic effects of acoustic streaming cause reverse flow to traveling waves.

ARTICLE INFO

Article history:
Received 22 January 2016
Received in revised form
13 January 2017
Accepted 5 February 2017
Available online xxxx

Keywords:
Peristaltic flow
Jeffrey fluid
MHD
Slip flow
Microchannel
Acoustics

ABSTRACT

The MHD peristaltic motion of a compressible and electrically conducting Jeffrey fluid induced by a surface acoustic wave in a confined parallel-plane microchannel through a porous medium is analytically investigated. A proper attention is given to the combined effects of physical parameters and magnetic field on the rheological aspects of the considered flow. The slip velocity is considered and the problem is discussed for free pumping case. The wave amplitude is related to the power output of an acoustic source. A perturbation technique is employed to analyze the problem in terms of a small amplitude ratio. In the second order approximation, the net axial velocity is calculated for various values of the fluid parameters. Finally, the effects of the parameters of interest on the mean axial velocity, the reversal flow, and the perturbation function are discussed and shown graphically. The critical value of the magnetic parameter M is discussed such that an optimum M is shown where some physical variables are obtained maximum. It is noticed that, for the Jeffrey fluid, oscillations decay rapidly as we move from the hydrodynamic to the hydromagnetic fluid, and the effect of retardation time becomes weak. It is inferred that increasing the magnetic parameter makes the fluid less prone to nonlinear effects. Several results of other fluid models are deduced as the limiting cases of our problem. This work is the most general model of peristalsis created to date with wide-ranging applications in biological microfluidic networks.

1. Introduction

The characteristics of fluid flow in microchannels have become the topic of extensive research lately with the rapid developments in industry. Several investigations have been undertaken to understand the variations between macro and microscale flows since microfluidic channels are utilized in many industrial applications such as micro-electric chip cooling, biomedical applications, and microelectro-mechanical systems [1–3]. Microfluidic channels, or tubes built in biomicroelectro-mechanical systems, are easily subjected to environment noises (oscillation or vibrations) and externally excited traveling waves (surface acoustic wave), where it is normally related to the peristaltic transport since the walls are flexible. These kinds of dynamic effects cannot be neglected when compressible fluids are flowing in such conduits [4,5]. Vafai and Khaled [6,7] analyzed the single and double layered flexible 2D microchannel heat sinks which have important applications in design and control of the flow.

Acoustic streaming has thus far been representing one of very few inertial phenomena that may actually play a considerable

* Corresponding author at: Basic Science Department, Faculty of Engineering, The British University in Egypt, Al-Shorouk City, Cairo 11837, Egypt.
E-mail addresses: siabdelsalam@engr.ucr.edu, siabdelsalam@caltech.edu, sara.abdelsalam@bue.edu.eg, siabdelsalam@yahoo.com (S.I. Abdelsalam).

http://dx.doi.org/10.1016/j.euromechflu.2017.02.002
0997-7546/

role in microfluidics. Due to the significant small sizes of the microfluidic devices, they prevent flow velocities from being high enough to yield high Reynolds numbers. However, acoustic waves of high frequency can circumvent such a difficulty. Although periodic wave motion might seem to be of small use to fluid manipulation, the inertial nonlinearity can rectify oscillatory fluid motion to give a time-averaged flow called acoustic streaming [8–11]. Chen [12] investigated the influence of ultrasonic radiation on the flow of water or oil through a stainless steel filter and on the flow of oil segments through a capillary. Chu [13] studied the flow induced by surface acoustic waves (SAW) in a microscale tube, and showed that the flow velocity of the gas is proportional to the second power of the SAW displacement velocity in these microchannels. Also, the effects of compressibility induced by SAW in a microchannel with compliant walls were studied by Mekheimer and Abdel-Wahab [14].

The key quantity in the study of microchannels is Knudsen number (K_n), which is the ratio between molecular mean free path to the representative physical length scale ($=A/l$). In fact, Knudsen number is very small for continuum flows. However, for gas flows in microdomains, the gas mean free path becomes comparable with the characteristic dimension of the conduit and K_n is greater than 0.001, and thus, the continuum approach assumption of fluid mechanics would no longer be a good approximation. A classification of different flow regimes in microchannels based on K_n shall be given later on [15,16].

There are two types of motions in the body of living organism; involuntary and voluntary. Both motions are characterized by muscular movements stimulated by nerve cells, yet the involuntary movement cannot be controlled by the will of organism himself. Normally in the human body, the peristaltic motion is an example of an involuntary wavelike contractions and relaxations of cardiac and smooth muscles. It occurs in transport tubes such as the oesophagus, urine transport from kidney to bladder or in some blood vessels [17–21]. Vafai et al. [22] studied the effect of Hall current and heat transfer on the peristaltic transport of a third grade fluid. Hayat et al. investigated the peristaltic transport for a compressible and incompressible Jeffrey fluid in a conduit with compliant walls [23,24].

Biological tissues are viscoelastic materials; their behavior is both viscous and elastic. A viscoelastic material possesses characteristics of stress-relaxation, creep, strain-rate sensitivity, and hysteresis [25]. The new ontology of nonlinear viscoelasticity enables a better understanding of biological materials by improving the ability to distinguish between different materials and providing insight into the physical mechanisms that cause material response [26,8,1]. Biological tissues generally contain blood vessels which can be categorized as vascular regions, one of which, stenosed artery through which the hyperthermia was analyzed in [27]. The characteristics of bioheat transfer through annular region were given by Wang et al. [28]. Gao and Jian [29] studied the MHD flow of the Jeffrey fluid in a circular microchannel taking the retardation time smaller than the relaxation time. Mekheimer et al. [4] investigated the peristaltic transport for a compressible Maxwell model in the presence of magnetic field where the wave amplitude was related to the power output of an acoustic source. Hayat et al. [30] gave a thorough analysis comparing the viscoelastic properties of Maxwell and Jeffrey fluids. Flow through a porous medium has been of considerable interest in recent years particularly among geophysical fluid dynamicists. A basic introduction is given by Aarts and Ooms, and Chen in [9,12], respectively. More comprehensive treatments can be found in [26,31], and detailed reviews are given by Elkoumy et al. [32].

The above mentioned investigations and existing literature on the peristaltic flows show that only few attempts study the peristaltic flows of compressible fluid. The most general study

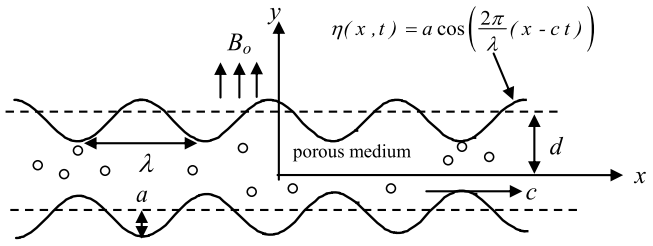

Fig. 1. Schematic showing the flow domain and its geometrical parameters.

of stimulation of compressible fluid flow in porous media via peristaltic mechanism is presented in [9]. The combined effect of a weakly compressible non-Newtonian fluid with wall slip on peristaltic flow has recently been investigated by Damianou and Georgiou [33]. Mekheimer and Abdel-Wahab investigated the peristaltic flow of a compressible Newtonian fluid through the microchannel and via the annulus in [14,5], respectively. However these studies did not take into account the effect of magnetic field on the flow properties. In fact, magnetohydrodynamic flows of fluids in conduits with elastic, rhythmically contracting walls (peristaltic flow) is of interest in connection with certain problems of the movement of conductive physiological fluids. Mekheimer et al. [4] extended the analysis of Ref. [14] to include the effects of the relaxation time of a Maxwell fluid together with the magnetic field in a microchannel. It was shown that there is a possibility of a fluid flow in the direction opposite to the propagation of the traveling wave. Elkoumy et al. [32] investigated the effect of strong magnetic field with Hall effect on the peristaltic flow of a Maxwell fluid in a channel. Recently, the MHD flow of an incompressible Jeffrey fluid in a circular microchannel has been studied in [29].

Nevertheless, the aforementioned investigations did not take into consideration the combined effect of magnetic field with viscoelastic parameters on the flow, and to the best of the authors' knowledge, this has not been done in the open literature. Under the purview of the present study, the aim of this article is to extend our interest in studying the arisen effects generated by introducing constant magnetic field and rheological properties in a microdomian of which the wave amplitude is related to the power output of an acoustic source. We suppose that the porous medium constitutes a compressible fluid which is originally stationary. That is, the zeroth-order pressure gradient is neglected at the beginning. Since the motion of MHD fluid across the magnetic field induces electric currents which change the magnetic field and the flow of the fluid, our work can help in better understanding of the behavior of complex nonlinear viscoelastic properties of biomaterials in MHD.

2. Formulation of the problem

A viscous, compressible, and electrically conducting Jeffrey fluid in a 2D symmetric channel of uniform width $2d$ is considered as shown in Fig. 1. The flow in the porous space is due to sinusoidal small-amplitude traveling waves on the flexible walls of the channel. A uniform magnetic field B_o is acting along the y-axis and the induced magnetic field is assumed negligible. We introduce the Cartesian coordinate system with the x-axis along the centerline of the channel and the y-axis normal to it. Let u and v denote the velocity components along x- and y-directions, respectively.

The flow is governed by the continuity equation

$$\frac{\partial \rho}{\partial t} + (\mathbf{V}\cdot\nabla\rho) + \rho(\nabla\cdot\mathbf{V}) = 0, \quad (1)$$

and the equations of motion

$$\rho\frac{\partial \mathbf{V}}{\partial t} + \rho(\mathbf{V}.\nabla)\mathbf{V} = -\nabla p + \nabla\cdot\mathbf{S} + \mathbf{R} + \mathbf{J}\times\mathbf{B} + \frac{\mu}{3}\nabla(\nabla\cdot\mathbf{V}), \quad (2)$$

Please cite this article in press as: S.I. Abdelsalam, K. Vafai, Combined effects of magnetic field and rheological properties on the peristaltic flow of a compressible fluid in a microfluidic channel, European Journal of Mechanics B/Fluids (2017), http://dx.doi.org/10.1016/j.euromechflu.2017.02.002

where ρ, t, p, μ are the density of fluid, time, interaction pressure due to the motion of fluid on the wall, and the dynamic viscosity, respectively. **V**, **J**, and **B** are the velocity vector, electric current density, and magnetic induction vector, respectively.

The constitutive equation of the extra stress tensor **S** for the Jeffrey fluid is defined as

$$\left(1+\lambda_1\frac{\partial}{\partial t}\right)\mathbf{S}=\mu\left(1+\lambda_2\frac{\partial}{\partial t}\right)\mathbf{A}_1, \tag{3a}$$

where λ_1 and λ_2 are the relaxation time and retardation time, respectively. The first Rivlin–Ericksen tensor $\mathbf{A}_1$ is defined by

$$\mathbf{A}_1=(\text{grad}\,\mathbf{V})+(\text{grad}\,\mathbf{V})^{\mathrm{T}}. \tag{3b}$$

On the basis of Jeffery fluid model, the following expression of Darcy's resistance **R** has been suggested [34]:

$$\left(1+\lambda_1\frac{\partial}{\partial t}\right)\mathbf{R}=-\frac{\mu\,\Phi}{K}\left(1+\lambda_2\frac{\partial}{\partial t}\right)\mathbf{V}, \tag{4}$$

where Φ $(0<\Phi<1)$, $K(>0)$ are, respectively, the (constant) porosity and permeability of the porous medium. The conducting fluid is permeated by an imposed uniform magnetic field B_0 which acts in the transverse direction. For low magnetic Reynolds number, the induced magnetic field can be ignored, the magnetic body force $\mathbf{J}\times\mathbf{B}$ becomes $\sigma(\mathbf{V}\times\mathbf{B})\times\mathbf{B}$ when imposed, induced electric fields are negligible, and only the magnetic field **B** contributes to the current $\mathbf{J}=\sigma(\mathbf{V}\times\mathbf{B})$. Here, σ is the electrical conductivity of the fluid.

The characteristic response of the fluid to compression is described by the constitutive equation

$$\frac{1}{\rho}\frac{\partial\rho}{\partial p}=k_c, \tag{5}$$

where k_c is the compressibility of the liquid. The solution of Eq. (5) for the density as a function of the pressure is given by

$$\rho=\rho_o\,\exp(k_c(p-p_c)), \tag{6}$$

where ρ_o is the (constant) density at the reference pressure p_c.

The continuity equation and the x- and y- equations of Eq. (2) are

$$\frac{\partial\rho}{\partial t}+u\frac{\partial\rho}{\partial x}+v\frac{\partial\rho}{\partial y}+\rho\left(\frac{\partial u}{\partial x}+\frac{\partial v}{\partial y}\right)=0, \tag{7}$$

$$\begin{aligned}&\left(1+\lambda_1\frac{\partial}{\partial t}\right)\left[\rho\left(\frac{\partial u}{\partial t}+u\frac{\partial u}{\partial x}+v\frac{\partial u}{\partial y}\right)\right]\\&=-\left(1+\lambda_1\frac{\partial}{\partial t}\right)\frac{\partial p}{\partial x}\\&\quad+\mu\left(1+\lambda_2\frac{\partial}{\partial t}\right)\left[\nabla^2u+\frac{1}{3}\frac{\partial}{\partial x}\left(\frac{\partial u}{\partial x}+\frac{\partial v}{\partial y}\right)\right]\\&\quad-\sigma B_o^2\left(1+\lambda_1\frac{\partial}{\partial t}\right)u-\frac{\mu\,\Phi}{K}\left(1+\lambda_2\frac{\partial}{\partial t}\right)u,\end{aligned} \tag{8}$$

$$\begin{aligned}&\left(1+\lambda_1\frac{\partial}{\partial t}\right)\left[\rho\left(\frac{\partial v}{\partial t}+u\frac{\partial v}{\partial x}+v\frac{\partial v}{\partial y}\right)\right]\\&=-\left(1+\lambda_1\frac{\partial}{\partial t}\right)\frac{\partial p}{\partial y}+\mu\left(1+\lambda_2\frac{\partial}{\partial t}\right)\\&\quad\times\left[\nabla^2v+\frac{1}{3}\frac{\partial}{\partial y}\left(\frac{\partial u}{\partial x}+\frac{\partial v}{\partial y}\right)\right]-\frac{\mu\,\Phi}{K}\left(1+\lambda_2\frac{\partial}{\partial t}\right)v,\end{aligned} \tag{9}$$

where x and y are the Cartesian coordinates with x measured in the direction of wave propagation and y measured in the direction normal to the mean position of the walls.

Let the vertical displacements of the upper and lower walls be η and $-\eta$, respectively, such that

$$\eta(x,t)=a\cos\left(\frac{2\pi}{\lambda}(x-ct)\right), \tag{10}$$

where a is the amplitude, λ is the wave length, and c is the wave speed. The horizontal displacement will be assumed zero. The appropriate boundary conditions are

$$u(x,\ \pm d\pm\eta,t)=\mp A\frac{\partial u}{\partial y}, \tag{11}$$

$$v(x,\pm d\pm\eta,t)=\pm\frac{\partial\eta\,(x,t)}{\partial t}. \tag{12}$$

Introducing the nondimensional variables and parameters where c and d are the characteristics velocity and length:

$$\begin{aligned}&x^*=\frac{x}{d},\quad y^*=\frac{y}{d},\quad \eta^*=\frac{\eta}{d},\quad u^*=\frac{u}{c},\\&v^*=\frac{v}{c},\quad \rho^*=\frac{\rho}{\rho_o},\\&t^*=\frac{ct}{d},\quad W^*=\frac{W}{d^2},\quad p^*=\frac{p}{\rho_o\,c^2},\\&p_c^*=\frac{p_c}{\rho_o\,c^2},\quad \tau^*=\frac{\tau c}{d}.\end{aligned} \tag{13}$$

The dimensionless parameters are given by

$$\varepsilon=\frac{a}{d},\quad \alpha=\frac{2\pi d}{\lambda},\quad R=\frac{\rho_o\,c\,d}{\mu},$$

$$\chi=k_c\rho_oc^2,\quad K_n=\frac{A}{d},\quad \text{and}\quad M=\frac{d\sigma}{\rho_o\,c}B_o^2$$

which represent the amplitude ratio, wave number, Reynolds number, compressibility parameter, slip parameter, and the magnetic parameter, respectively.

In terms of these variables, Eqs. (6)–(12) reduce to

$$\rho=\exp(\chi(p-p_c)), \tag{14}$$

$$\frac{\partial\rho}{\partial t}+u\frac{\partial\rho}{\partial x}+v\frac{\partial\rho}{\partial y}+\rho\left(\frac{\partial u}{\partial x}+\frac{\partial v}{\partial y}\right)=0, \tag{15}$$

$$\begin{aligned}&\left(1+\lambda_1\frac{\partial}{\partial t}\right)\left[\rho\left(\frac{\partial u}{\partial t}+u\frac{\partial u}{\partial x}+v\frac{\partial u}{\partial y}\right)\right]\\&=-\left(1+\lambda_1\frac{\partial}{\partial t}\right)\frac{\partial p}{\partial x}+\frac{1}{R}\left(1+\lambda_2\frac{\partial}{\partial t}\right)\\&\quad\times\left[\nabla^2u+\frac{1}{3}\frac{\partial}{\partial x}\left(\frac{\partial u}{\partial x}+\frac{\partial v}{\partial y}\right)\right]\\&\quad-M\left(1+\lambda_1\frac{\partial}{\partial t}\right)u-\frac{1}{K}\left(1+\lambda_2\frac{\partial}{\partial t}\right)u,\end{aligned} \tag{16}$$

$$\begin{aligned}&\left(1+\lambda_1\frac{\partial}{\partial t}\right)\left[\rho\left(\frac{\partial v}{\partial t}+u\frac{\partial v}{\partial x}+v\frac{\partial v}{\partial y}\right)\right]\\&=-\left(1+\lambda_1\frac{\partial}{\partial t}\right)\frac{\partial p}{\partial y}+\frac{1}{R}\left(1+\lambda_2\frac{\partial}{\partial t}\right)\\&\quad\times\left[\nabla^2v+\frac{1}{3}\frac{\partial}{\partial y}\left(\frac{\partial u}{\partial x}+\frac{\partial v}{\partial y}\right)\right]-\frac{1}{K}\left(1+\lambda_2\frac{\partial}{\partial t}\right)v,\end{aligned} \tag{17}$$

$$\eta=\varepsilon\,\cos\,\alpha\,(x-t), \tag{18}$$

$$u=\mp K_n\frac{\partial u}{\partial y}\quad\text{at}\,y=\pm1\pm\eta, \tag{19}$$

$$v=\pm\frac{\partial\eta}{\partial t}\quad\text{at}\,y=\pm1\pm\eta \tag{20}$$

in which the asterisks have been suppressed for simplicity.

Please cite this article in press as: S.I. Abdelsalam, K. Vafai, Combined effects of magnetic field and rheological properties on the peristaltic flow of a compressible fluid in a microfluidic channel, European Journal of Mechanics B/Fluids (2017), http://dx.doi.org/10.1016/j.euromechflu.2017.02.002

3. Solution development

To solve the system of Eqs. (14)–(17), we first take the steady parallel flow case in which $u = u_o(y)$ and $v = 0$. So that under the effect of constant pressure gradient $\partial p/\partial x = \partial p_o/\partial x =$ constant, the solution of the system will be

$$u_o(y) = \frac{R}{\delta^2}\frac{dp_o}{dx}\frac{(\cosh\delta y - \cosh\delta - K_n\delta\sinh\delta)}{(\cosh\delta + K_n\delta\sinh\delta)}, \tag{21}$$

with $\delta = \sqrt{M\,R + R/K}$.

And for the no-slip condition, we have $K_n \to 0$ and so

$$u_o(y) = \frac{R}{\delta^2}\frac{dp_o}{dx}\frac{(\cosh\delta\, y - \cosh\delta)}{\cosh\delta}. \tag{22}$$

This mean flow depends on the physical quantities relevant to the motion of the system [4]. In the steady state case, peristaltic mean flow is created by the traveling wave motion in the wall. The free pumping case, $\partial p_o/\partial x = 0$, is known as the pure peristalsis case [19]. We assume the pressure, the velocity components, and the density in the form:

$$\begin{aligned}
p &= p_o + \varepsilon p_1(x,y,t) + \varepsilon^2 p_2(x,y,t) + \cdots,\\
u &= \varepsilon\, u_1(x,y,t) + \varepsilon^2 u_2(x,y,t) + \cdots,\\
v &= \varepsilon v_1(x,y,t) + \varepsilon^2 v_2(x,y,t) + \cdots,\\
\rho &= 1 + \varepsilon\,\rho_1(x,y,t) + \varepsilon^2\rho_2(x,y,t) + \cdots.
\end{aligned} \tag{23}$$

Substituting the expansions (23) in (14)–(17) and equating the coefficients of equal powers of ε on both sides of the equations, we obtain: for ε

$$\begin{aligned}
&\rho_1 = \chi p_1, \quad \frac{\partial\rho_1}{\partial t} + \frac{\partial u_1}{\partial x} + \frac{\partial v_1}{\partial y} = 0,\\
&\left(1+\lambda_1\frac{\partial}{\partial t}\right)\frac{\partial u_1}{\partial t}\\
&\quad = -\left(1+\lambda_1\frac{\partial}{\partial t}\right)\frac{\partial p_1}{\partial x} + \frac{1}{R}\left(1+\lambda_2\frac{\partial}{\partial t}\right)\\
&\qquad\times\left[\left(\frac{\partial^2 u_1}{\partial x^2} + \frac{\partial^2 u_1}{\partial y^2}\right) + \frac{1}{3}\frac{\partial}{\partial x}\left(\frac{\partial u_1}{\partial x} + \frac{\partial v_1}{\partial y}\right)\right]\\
&\qquad - M\left(1+\lambda_1\frac{\partial}{\partial t}\right)u_1 - \frac{1}{K}\left(1+\lambda_2\frac{\partial}{\partial t}\right)u_1,\\
&\left(1+\lambda_1\frac{\partial}{\partial t}\right)\frac{\partial v_1}{\partial t}\\
&\quad = -\left(1+\lambda_1\frac{\partial}{\partial t}\right)\frac{\partial p_1}{\partial y} + \frac{1}{R}\left(1+\lambda_2\frac{\partial}{\partial t}\right)\\
&\qquad\times\left[\left(\frac{\partial^2 v_1}{\partial x^2} + \frac{\partial^2 v_1}{\partial y^2}\right) + \frac{1}{3}\frac{\partial}{\partial y}\left(\frac{\partial u_1}{\partial x} + \frac{\partial v_1}{\partial y}\right)\right]\\
&\qquad - \frac{1}{K}\left(1+\lambda_2\frac{\partial}{\partial t}\right)v_1.
\end{aligned} \tag{24}$$

For ε^2:

$$\begin{aligned}
&\rho_2 = \chi p_2 + \frac{1}{2}\chi^2 p_1^2,\\
&\frac{\partial\rho_2}{\partial t} + u_1\frac{\partial\rho_1}{\partial x} + v_1\frac{\partial\rho_1}{\partial y} + \frac{\partial u_2}{\partial x} + \frac{\partial v_2}{\partial y}\\
&\quad + \rho_1\left(\frac{\partial u_1}{\partial x} + \frac{\partial v_1}{\partial y}\right) = 0,\\
&\left(1+\lambda_1\frac{\partial}{\partial t}\right)\left(\frac{\partial u_2}{\partial t} + u_1\frac{\partial u_1}{\partial x} + v_1\frac{\partial u_1}{\partial y} + \rho_1\frac{\partial u_1}{\partial t}\right)\\
&\quad = -\left(1+\lambda_1\frac{\partial}{\partial t}\right)\frac{\partial p_2}{\partial x} + \frac{\left(1+\lambda_2\frac{\partial}{\partial t}\right)}{R}\\
&\qquad\times\left(\frac{\partial^2 u_2}{\partial x^2} + \frac{\partial^2 u_2}{\partial y^2} + \frac{1}{3}\frac{\partial}{\partial x}\left(\frac{\partial u_2}{\partial x} + \frac{\partial v_2}{\partial y}\right)\right)\\
&\qquad - M\left(1+\lambda_1\frac{\partial}{\partial t}\right)u_2 - \frac{\left(1+\lambda_2\frac{\partial}{\partial t}\right)}{K}u_2,\\
&\left(1+\lambda_1\frac{\partial}{\partial t}\right)\left(\frac{\partial v_2}{\partial t} + u_1\frac{\partial v_1}{\partial x} + v_1\frac{\partial v_1}{\partial y} + \rho_1\frac{\partial v_1}{\partial t}\right)\\
&\quad = -\left(1+\lambda_1\frac{\partial}{\partial t}\right)\frac{\partial p_2}{\partial y} + \frac{\left(1+\lambda_2\frac{\partial}{\partial t}\right)}{R}\\
&\qquad\times\left(\frac{\partial^2 v_2}{\partial x^2} + \frac{\partial^2 v_2}{\partial y^2} + \frac{1}{3}\frac{\partial}{\partial y}\left(\frac{\partial u_2}{\partial x} + \frac{\partial v_2}{\partial y}\right)\right)\\
&\qquad - \frac{\left(1+\lambda_2\frac{\partial}{\partial t}\right)}{K}v_2,
\end{aligned} \tag{25}$$

etc.

We represent the boundary conditions given by Eqs. (19) and (20) by a Taylor expansion around $y = \pm 1$, then we substitute these expansions into the boundary conditions, and with the aid of Eq. (23), we express cosines and sines in exponential powers. These yield: for ε

$$u_1(x,\pm1,\,t) = \mp K_n\, u_{1y}(x,\pm1,t), \tag{26}$$

$$v_1(x,\pm1,\,t) = \mp\frac{i\alpha}{2}(e^{i\alpha(x-t)} - e^{-i\alpha(x-t)}). \tag{27}$$

And for ε^2:

$$\begin{aligned}
&u_2(x,\pm1,\,t) \pm \frac{1}{2}(e^{i\alpha(x-t)} + e^{-i\alpha(x-t)})\,u_{1y}(x,\pm1,t)\\
&\quad = \mp K_n\left[u_{2y}(x,\pm1,\,t) \pm \frac{1}{2}(e^{i\alpha(x-t)}\right.\\
&\qquad \left. + e^{-i\alpha(x-t)})\,u_{1yy}(x,\pm1,\,t)\right],
\end{aligned} \tag{28}$$

$$v_2(x,\pm1,\,t) \pm \frac{1}{2}(e^{i\alpha(x-t)} + e^{-i\alpha(x-t)})v_{1y}(x,\pm1,t) = 0. \tag{29}$$

We seek a solution in the form

$$\begin{aligned}
u_1(x,y,\,t) &= U_1(y)\,e^{i\alpha(x-t)} + \overline{U}_1(y)\,e^{-i\alpha(x-t)},\\
v_1(x,y,\,t) &= V_1(y)\,e^{i\alpha(x-t)} + \overline{V}_1(y)\,e^{-i\alpha(x-t)},\\
p_1(x,y,\,t) &= P_1(y)\,e^{i\alpha(x-t)} + \overline{P}_1(y)\,e^{-i\alpha(x-t)},\\
\rho_1(x,y,\,t) &= \chi P_1(y)\,e^{i\alpha(x-t)} + \chi\overline{P}_1(y)\,e^{-i\alpha(x-t)},
\end{aligned} \tag{30}$$

and

$$\begin{aligned}
u_2(x,y,\,t) &= U_{20}(y) + U_2(y)\,e^{2i\alpha(x-t)} + \overline{U}_2(y)\,e^{-2i\alpha(x-t)},\\
v_2(x,y,\,t) &= V_{20}(y) + V_2(y)\,e^{2i\alpha(x-t)} + \overline{V}_2(y)\,e^{-2i\alpha(x-t)},\\
p_2(x,y,\,t) &= P_{20}(y) + P_2(y)\,e^{2i\alpha(x-t)} + \overline{P}_2(y)\,e^{-2i\alpha(x-t)},\\
\rho_2(x,y,\,t) &= D_{20}(y) + D_2(y)\,e^{2i\alpha(x-t)} + \overline{D}_2(y)\,e^{-2i\alpha(x-t)}
\end{aligned} \tag{31}$$

where the overbar denotes the complex conjugate of the variable.

Substituting the assumed solutions, (30) and (31), into (24) through (29), we obtain the following sets of first-order and second-order equations, respectively:

$$\begin{aligned}
&V_1' + i\,\alpha\,U_1 = i\,\alpha\,\chi\,P_1,\\
&-i\,\alpha\,\gamma^*\,U_1 \;=\; -i\,\alpha\,\gamma^*\,P_1 + \frac{1}{R}\left[U_1'' - \left(\alpha^2 + \frac{R}{K} + M\,R\gamma^*\right)U_1\right]\\
&\qquad\qquad + \frac{i\,\alpha}{3\,R}\left(V_1' + i\,\alpha\,U_1\right),
\end{aligned}$$

Please cite this article in press as: S.I. Abdelsalam, K. Vafai, Combined effects of magnetic field and rheological properties on the peristaltic flow of a compressible fluid in a microfluidic channel, European Journal of Mechanics B/Fluids (2017), http://dx.doi.org/10.1016/j.euromechflu.2017.02.002

$$-i\alpha\,\gamma^{*}\,V_1 \;=\; -\gamma^{*}\,P_1' + \frac{1}{R}\left[V_1'' - \left(\alpha^2 + \frac{R}{K}\right)V_1\right] + \frac{1}{3R}\frac{d}{dy}\left(V_1' + i\alpha\,U_1\right),$$

$$U_1(\pm 1) = \mp K_n\,U_1'(\pm 1), \qquad V_1(\pm 1) = \mp\frac{i\alpha}{2}, \tag{32}$$

and

$$D_{20} = \chi\,P_{20} + \chi^2\,\overline{P_1}\,P_1,$$

$$-P_{20}' + \frac{4}{3R}\,V_{20}'' - \frac{1}{K}\,V_{20} \;=\; i\alpha\,\chi\,P_1\,\overline{V_1} - i\alpha\,\overline{P_1}\,V_1 + V_1\,\overline{V_1'} + V_1'\,\overline{V_1} - i\alpha\,U_1\,\overline{V_1} + i\alpha\,\overline{U_1}\,V_1,$$

$$\frac{1}{R}U_{20}'' - \left(\frac{1}{K} + M\right)U_{20} = i\alpha\,\chi\,\overline{U_1}\,P_1 - i\alpha\,\chi\,\overline{P}_1\,U_1 + V_1\,\overline{U_1'} + \overline{V_1}\,U_1',$$

$$V_{20}' = -\chi\,\left(P_1\,\overline{V_1'} + \overline{P}_1\,V_1' + V_1\,\overline{P_1'} + \overline{V_1}\,P_1'\right),$$

$$U_{20}(\pm 1) \pm \frac{1}{2}\left(\overline{U_1'}(\pm 1) + U_1'(\pm 1)\right) = \mp K_n\left[U_{20}'(\pm 1) \pm \frac{1}{2}\left(\overline{U_1''}(\pm 1) + U_1''(\pm 1)\right)\right],$$

$$V_{20}(\pm 1) \pm \frac{1}{2}\left(\overline{V_1'}(\pm 1) + V_1'(\pm 1)\right) = 0, \tag{33}$$

where the complex parameters are given by:

$$\gamma_1 = 1 - i\alpha\,\lambda_1, \qquad \gamma_2 = 1 - i\alpha\,\lambda_2, \qquad \gamma* = \frac{\gamma_1}{\gamma_2}.$$

Following the solution procedure introduced originally by Aarts and Ooms [9], and which was followed by Mekheimer et al. [4] afterwards, we repeat the same analysis and obtain the master equations. Thus, we omit the lengthy calculations and obtain the first-order solution for the velocity and pressure:

$$V_1(y) = C_1\,\sinh a_1 y + C_2\,\sinh a_2 y,$$
$$U_1(y) = b_1\,C_1\,\cosh a_1 y + b_2\,C_2\,\cosh a_2 y + C_3\chi,$$
$$P_1(y) = C_1\,\frac{(a_1^2 - \beta_1^2)}{\gamma a_1}\cosh a_1 y + C_2\,\frac{(a_2^2 - \beta_1^2)}{\gamma a_2}\cosh a_2 y + C_3. \tag{34}$$

Similarly, the solution to the second-order system (33) is developed as follows:

$$V_{20} = -\chi\,\left(P_1\,\overline{V_1} + \overline{P}_1\,V_1\right) + D_1,$$
$$U_{20}(y) = D_2\,\cosh\delta y + D_3\,\sinh\delta y + E(y),$$
$$P_{20}(y) = D_4 - \frac{4\chi}{3R}\,H(y) - \frac{1}{K}\int_{-1}^{y} V_{20}(r)\,dr - \int_{-1}^{y} F(r)\,dr. \tag{35}$$

Here, the complex constant D_4 follows from a given pressure $P_{20}(-1)$ on the microchannel wall. Also, the complex parameters and constants obtained in the solution are given in the Appendix.

The net axial velocity is considered over one period of time. The average of a variable g over one period T of time t is

$$\langle g\rangle \;=\; \frac{1}{T}\int_0^T g(x,y,t)\,dt, \tag{36}$$

where $T = 2\pi/\alpha$. The mean net axial velocity and the net flow rate are, respectively, given by

$$\langle u\rangle = \varepsilon^2\,U_{20}(y), \tag{37}$$

$$\langle Q\rangle = \varepsilon^2\int_0^1 U_{20}(y)\,dy. \tag{38}$$

4. Results and discussion

In this section, theoretical estimates of sundry physical quantities that are of relevance to the fluid problem have been obtained on the basis of the present analysis. We investigate novelties brought about by the introduction of the combination of the magnetic parameter M, the permeability parameter of the medium K, the relaxation time λ_1, the retardation time λ_2, the compressibility parameter χ, and the slip parameter K_n into the model. Particularly, we discuss their combined effects on the mean velocity at the boundaries D_{wall}, the mean velocity perturbation function G(y), the time-averaged mean axial velocity distribution, and the net flow rate. In the present study, all the graphical results are achieved using the Mathematica program. To be specific, we set the small parameter ($\varepsilon < 1$) because we have used the perturbation method with the amplitude ratio (ε) as a parameter.

Fig. 2(a) through (f) show the variations of $D_{\text{wall}}(=U_{20}(1))$ with the wave number α for various values of M, K, λ_1, λ_2, χ and K_n. In Fig. 2(a), it is noticed that D_{wall} increases as we move from the hydrodynamic to hydromagnetic fluid unlike the effect of K that is shown in Fig. 2(b). Fig. 2(c) depicts the variations of λ_1 in the presence and absence of M. It is observed that in the presence of $M(>1.5)$, λ_1 has an increasing effect on D_{wall}, while the effect becomes weak for $M = 1.5$. Furthermore, the effect of λ_1 is quite opposite for small values of $M(<1.5)$ where it has a decreasing effect on D_{wall} and which conforms to the results given by [23]. The possible reason is that the opposing magnetic field plays a significant role and exceeds the viscoelastic effects. It is also observed from Fig. 2(d) that in case of Jeffrey fluid, D_{wall} is much greater in magnitude than that of Maxwell fluid ($\lambda_2 = 0$). Also, there is a rapid increase in the values of D_{wall} which indicates that viscoelastic effects are more pronounced for large values of λ_2.

For the Knudsen number, the flow regimes can be divided into various regions. These are continuum, slip, transition, and free molecular flow regimes. If $K_n < 0.001$, the molecular mean free path of the molecules is negligible in comparison to the geometrical dimensions, and the fluid can be treated as a continuous medium. If $0.001 < K_n < 0.1$, it is found that the fluid loses grip on the boundaries and tends to slip along the walls of the domain. If $0.1 < K_n < 3.0$, it is transition flow regimes. Finally, the flow enters the free molecular regime when $K_n > 3.0$, each regime requires a particular type of analysis [17,18]. Fig. 2(e) and (f) depict that for any value of the wave number α, D_{wall} decreases with an increase in both values of χ and K_n. Moreover, Fig. 2(f) depicts that D_{wall} has more magnitude for nonslip flow when compared with the slip flow.

Following Fung and Yih [19], we define the mean velocity perturbation function G(y) as

$$\text{G}(y) = \frac{-200}{\alpha^2 R^2}[E(y) - E(1)].$$

Fig. 3(a)–(h) give insight into the changes in the behavior of G(y) with y that occur due to changes in the values of different parameters governing the flow. The critical value of M is discussed for MHD perturbation function and an optimum M is shown where G(y) is attained maximum. It is noticed in Fig. 3(a) that as a result of increasing the magnetic field, G(y) is reduced. The possible reason is that because of the force field that is given by the current $\mathbf{J}\times\mathbf{B}$ of Eq. (2) includes now only the opposing part (hindering force) with magnitude $\sigma B_0^2 u$, thus, the retarding force is dominant and the mean velocity perturbation function decreases. It is also noticed that the perturbed velocity tends to become flat with increasing M. The latter phenomenon is pronounced with higher values of M and shall be discussed subsequently. It is observed in Fig. 3(b) that K has an increasing effect on G(y) which in turn moves towards the wall asymptotically. Fig. 3(c) and (d) illustrate the variations

Please cite this article in press as: S.I. Abdelsalam, K. Vafai, Combined effects of magnetic field and rheological properties on the peristaltic flow of a compressible fluid in a microfluidic channel, European Journal of Mechanics B/Fluids (2017), http://dx.doi.org/10.1016/j.euromechflu.2017.02.002

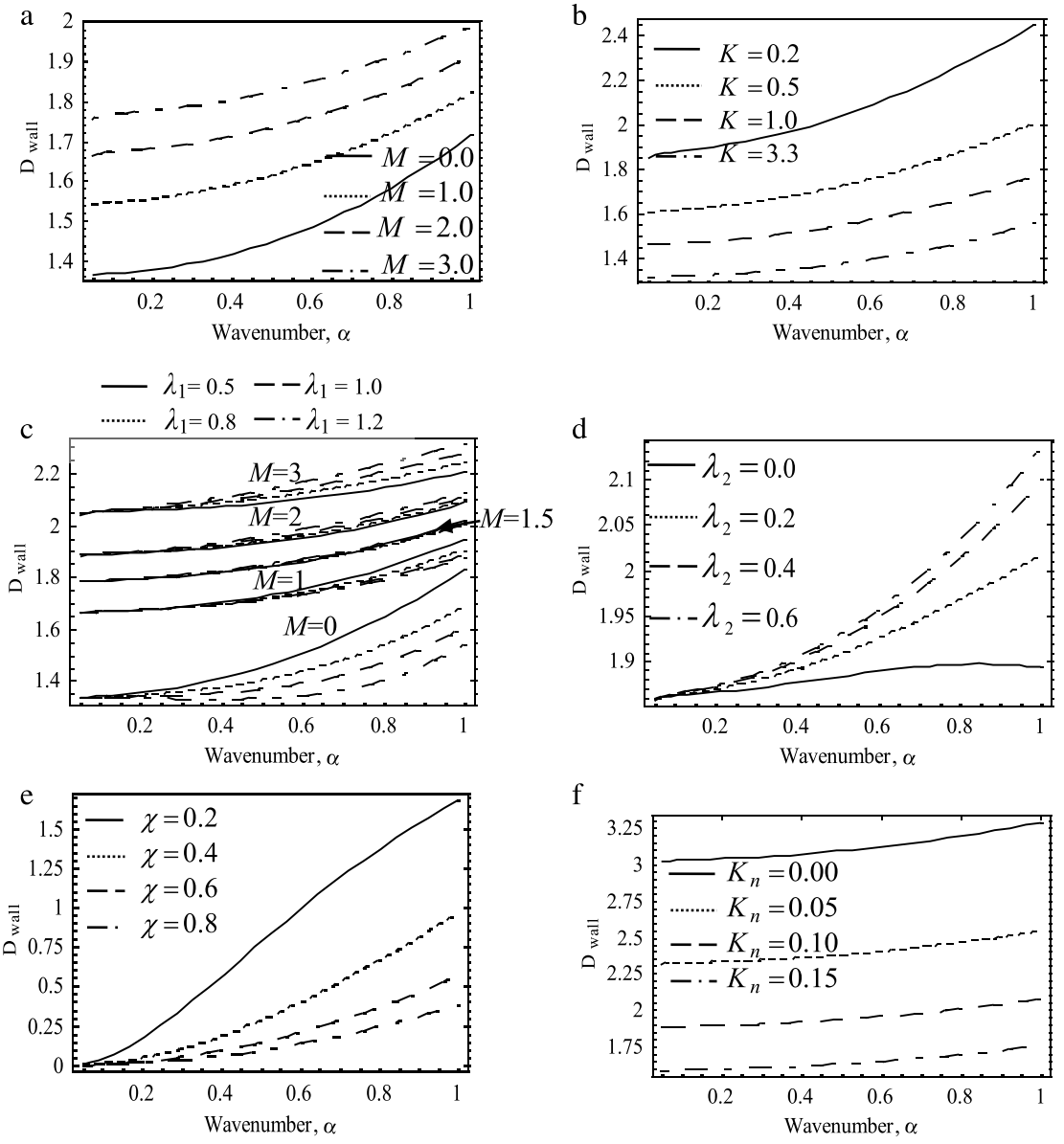

Fig. 2. The variation of D_{wall} with wavenumber α for: $K = 1$, $\lambda_1 = 0.7$, $\lambda_2 = 0.4$, $\chi = 0.001$, $K_n = 0.15$, and $R = 10$ (panel a); $M = 0.5$, $\lambda_1 = 0.7$, $\lambda_2 = 0.4$, $\chi = 0.001$, $K_n = 0.15$, and $R = 10$ (panel b); $M = 0, 1, 1.5, 2, 3$, $K = 3.3$, $K_n = 0.1$, $\chi = 0.001$, $\lambda_2 = 0.5$, and $R = 10$ (panel c); $M = 1.5$, $\chi = 0.001$, $K = 1.5$, $\lambda_1 = 0.8$, $K_n = 0.1$, and $R = 10$ (panel d); $M = 2$, $K = 1.5$, $K_n = 0.15$, $\lambda_1 = 0.7$, $\lambda_2 = 0.4$, and $R = 10$ (panel e); $M = 2$, $\chi = 0.001$, $K = 3.3$, $\lambda_1 = 0.7$, $\lambda_2 = 0.4$, and $R = 10$ (panel f).

of λ_1 in the presence and absence of M. It is observed in Fig. 3(c) that for $M = 0$, λ_1 has an increasing effect just like the results in [23], and then comes a separating point ($M = 0.15$) where λ_1 does not have a significant effect on G(y) from which G(y) starts to promptly decrease with λ_1 for $M > 0.15$ (Fig. 3(d)). Alternatively, Fig. 3(e) and (f) illustrate the combined effects of M and λ_2 on G(y). It is shown in Fig. 3(e) that $M = 0$ causes λ_2 to have a decreasing effect on the perturbation function till it reaches a critical value of M(=0.3) where λ_2 weakly affects G(y) (Fig. 3(f)). Afterwards, the behavior of G(y) dramatically changes to be increasing rapidly with λ_2 at higher values of M. It is also concluded that G(y) attains smaller values for a Maxwell fluid and increases for larger values of the retardation time as illustrated in Fig. 3(f). It is generally noticed in Fig. 3(a), (b), (d), and (f) that the flat effect is caused by the magnetic field and by higher values of Reynolds number ($R \geq 10$). In addition, G(y) attains the maximum value near the center of the channel and remains constant over a certain range of y.

Fig. 3(g) elucidates that for $M = 0$, G(y) is reduced with an increase in the values of χ till it reaches to a point ($M = 0.04$) where χ does not have a significant effect on it, then its behavior is reversed with χ for $M > 0.04$. Fig. 3(h) demonstrates that for a slip flow, the perturbation function moves towards the wall upstream and that the phenomenon is accelerated by the compressibility. Initially, the effect of the slip dependency prevails, but as χ is increased, these are counterbalanced and then suppressed by compressibility effect. Further, it is noticed that G(y) has less magnitude for the nonslip fluid when compared to the slip fluid.

Fig. 4(a)–(g) display the variations of the mean velocity distribution and reversal flow with y for various values of M, K, and λ_1. We heuristically consider the main changes introduced by the high magnetic field on the flow. In Fig. 4(a), a reversal of the velocity pattern is observed as the magnetic number is increased for $R = 1$. The significant change in the reflux region increases very fast due to the large values of M considered in the analysis. Fig. 4(b) and (c) demonstrate that at $R \geq 10$, the presence of magnetic field results in a deceleration in the possibility of the reversal flow till the influence of M almost vanishes in the centre

Please cite this article in press as: S.I. Abdelsalam, K. Vafai, Combined effects of magnetic field and rheological properties on the peristaltic flow of a compressible fluid in a microfluidic channel, European Journal of Mechanics B/Fluids (2017), http://dx.doi.org/10.1016/j.euromechflu.2017.02.002

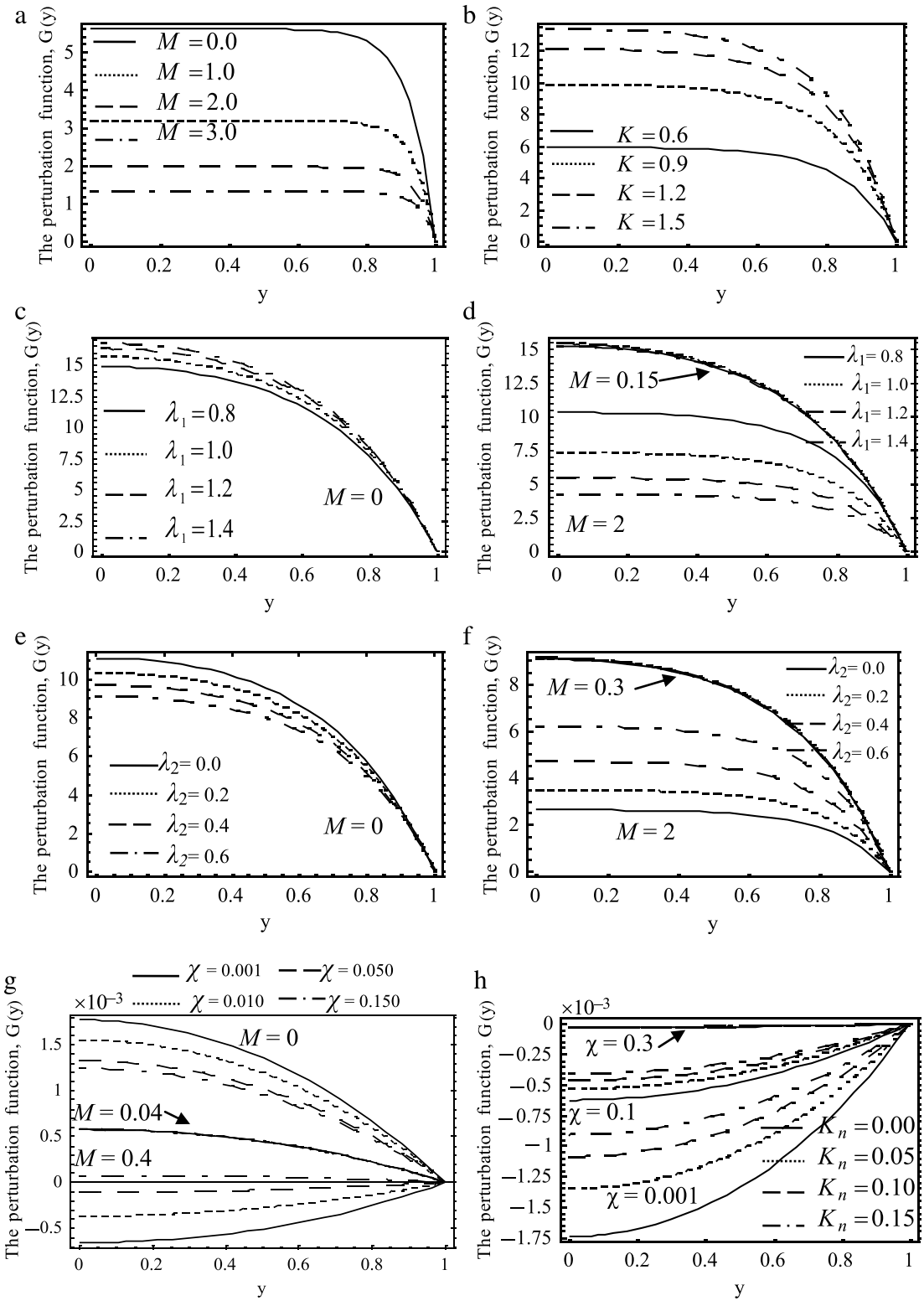

Fig. 3. The variation of the mean velocity perturbation function G(y) for: $K = 0.5$, $\lambda_1 = 0.7$, $\lambda_2 = 0.4$, $\chi = 0.1$, $K_n = 0.15$, $R = 100$, and $\alpha = 0.1$ (panel a); $M = 1.5$, $\lambda_1 = 0.7$, $\lambda_2 = 0.4$, $\chi = 0.4$, $K_n = 0.15$, $R = 15$, and $\alpha = 0.2$ (panel b); $M = 0$, $K = 1.5$, $\lambda_2 = 0.6$, $\chi = 0.3$, $K_n = 0.15$, $R = 10$, and $\alpha = 0.4$ (panel c); $M = 0.15$ (solid line), $M = 2$ (others), $K = 1.5$, $\lambda_2 = 0.6$, $\chi = 0.3$, $K_n = 0.15$, $R = 10$, and $\alpha = 0.4$ (panel d); $M = 0$, $K = 1.5$, $\lambda_1 = 0.7$, $\chi = 0.4$, $K_n = 0.15$, $R = 10$, and $\alpha = 0.5$ (panel e); $M = 0.3$ (solid line), $M = 2$ (others), $K = 1.5$, $\lambda_1 = 0.7$, $\chi = 0.4$, $K_n = 0.15$, $R = 10$, and $\alpha = 0.5$ (panel f); $M = 0$ (top), $M = 0.04$ (middle solid), $M = 0.4$ (bottom), $K = 1$, $\lambda_1 = 0.7$, $\lambda_2 = 0.5$, $K_n = 0.001$, $R = 1$, and $\alpha = 0.5$ (panel g); $\chi = 0.3$ (top), $\chi = 0.1$ (middle), $\chi = 0.001$ (bottom) $M = 1$, $K = 3.3$, $\lambda_1 = 0.5$, $\lambda_2 = 0.2$, $R = 1$, and $\alpha = 0.5$ (panel h).

of the channel causing a dramatic change in the nature of the mean velocity profile from parabolic to flat structure. This phenomenon is rather clarified by taking a snapshot for the 3D velocity contour pattern as seen in Fig. 4(d) and (e). It is shown that when the applied magnetic field is in transverse direction, the mean velocity distribution is dependent upon Reynolds number. That is, for low

Please cite this article in press as: S.I. Abdelsalam, K. Vafai, Combined effects of magnetic field and rheological properties on the peristaltic flow of a compressible fluid in a microfluidic channel, European Journal of Mechanics B/Fluids (2017), http://dx.doi.org/10.1016/j.euromechflu.2017.02.002

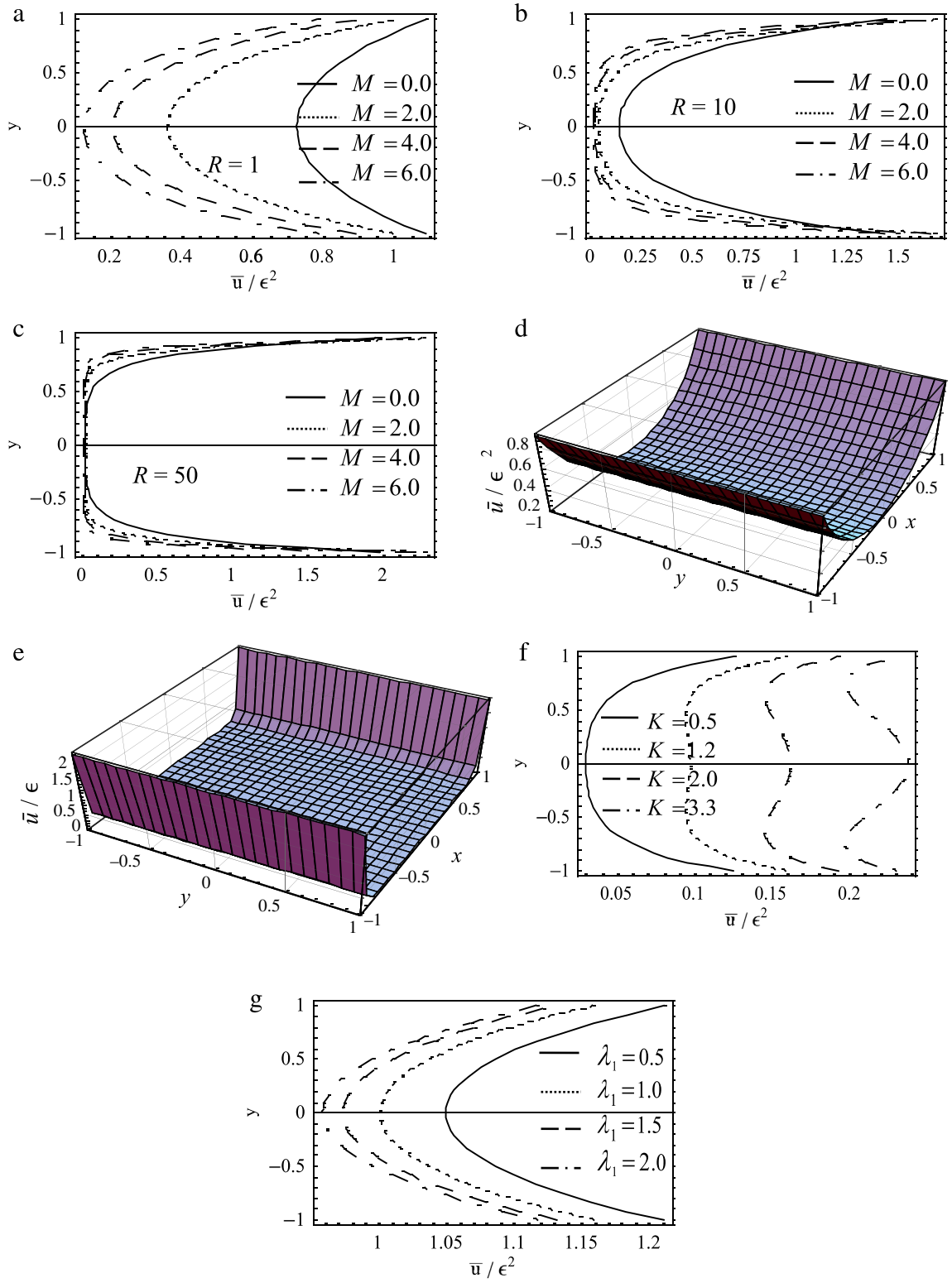

Fig. 4. The variation of the mean-axial velocity distribution for: $K = 1$, $\lambda_1 = 1.2$, $\lambda_2 = 0.5$, $\chi = 0.05$, $K_n = 0.15$, $R = 1$, and $\alpha = 0.5$ (panel a); $K = 1$, $\lambda_1 = 1.2$, $\lambda_2 = 0.5$, $\chi = 0.05$, $K_n = 0.15$, $R = 10$, and $\alpha = 0.5$ (panel b); $K = 1$, $\lambda_1 = 1.2$, $\lambda_2 = 0.5$, $\chi = 0.05$, $K_n = 0.15$, $R = 50$, and $\alpha = 0.5$ (panel c); $M = 4$, $K = 1$, $\lambda_1 = 1.2$, $\lambda_2 = 0.5$, $\chi = 0.05$, $K_n = 0.15$, $R = 1$, and $\alpha = 0.5$ (panel d); $M = 4$, $K = 1$, $\lambda_1 = 1.2$, $\lambda_2 = 0.5$, $\chi = 0.05$, $K_n = 0.15$, $R = 100$, and $\alpha = 0.5$ (panel e); $M = 0.2$, $\lambda_1 = 0.7$, $\lambda_2 = 0.4$, $\chi = 0.9$, $K_n = 0.15$, $R = 5$, and $\alpha = 0.5$ (panel f); $M = 0.05$, $K = 3.3$, $\lambda_2 = 0.5$, $\chi = 0.05$, $K_n = 0.15$, $R = 1$, and $\alpha = 0.5$ (panel g).

Reynolds number, the velocity still preserve its parabolic nature where the largest values are reached in the surroundings of $y = 0$ plane, but for higher values of R, the flat structure is noticed and the mirror symmetry is maintained. Fig. 4(f) shows that the mean flow decreases with an increase in K but increases when $K \geq 2$ and this happens because the permeability parameter allows more fluid to pass through the pores. Thus, the more the permeability will be, the more the velocity of fluid. Fig. 4(g) reveal that upon increasing λ_1, a backward flow in the neighborhood of the center line occurs, and the mean axial velocity increases in the reversal flow.

Please cite this article in press as: S.I. Abdelsalam, K. Vafai, Combined effects of magnetic field and rheological properties on the peristaltic flow of a compressible fluid in a microfluidic channel, European Journal of Mechanics B/Fluids (2017), http://dx.doi.org/10.1016/j.euromechflu.2017.02.002

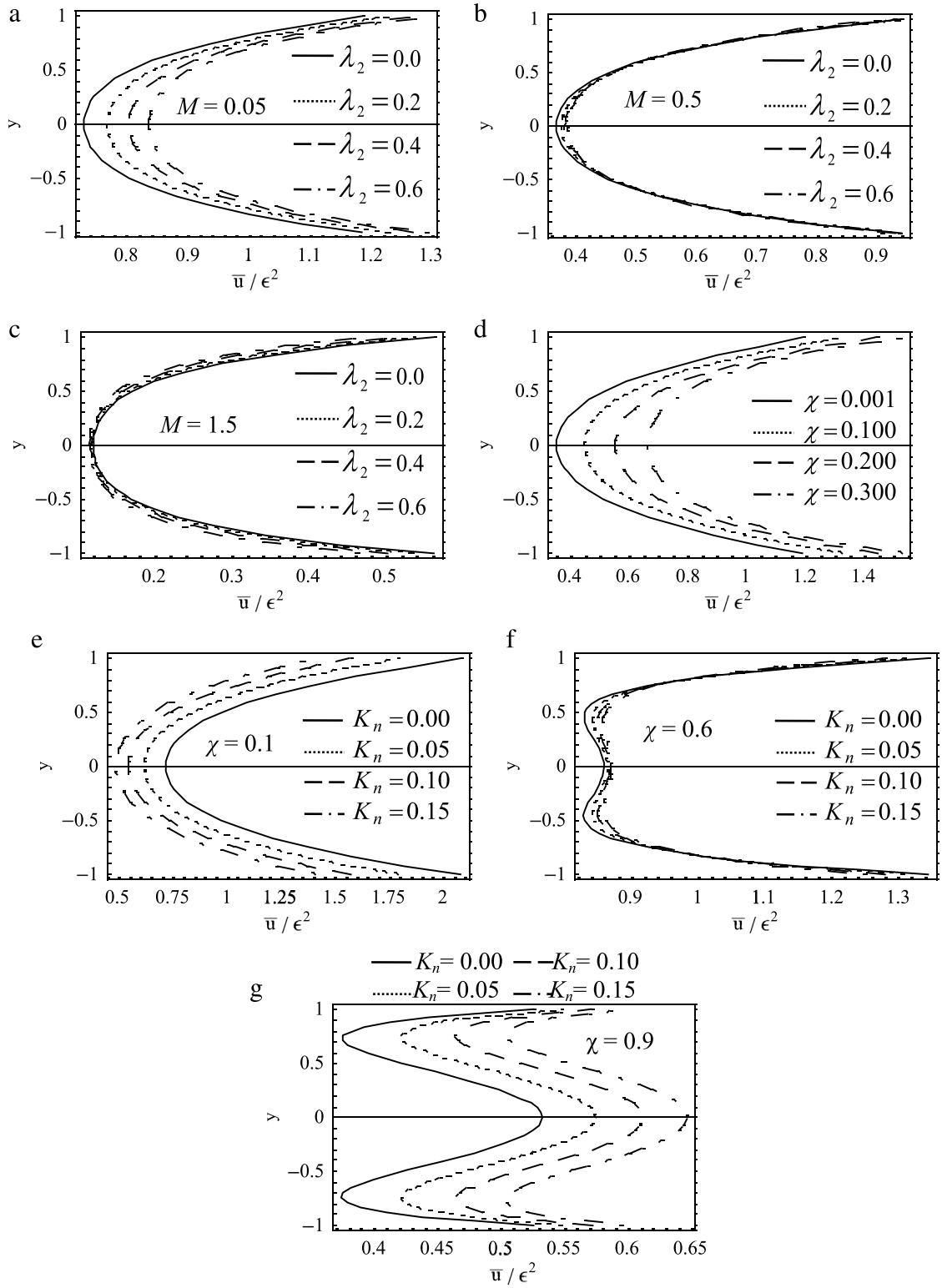

Fig. 5. The variation of the mean-axial velocity distribution for: $M = 0.05$, $K = 3.3$, $\lambda_1 = 0.7$, $\chi = 0.3$, $K_n = 0.15$, $R = 5$, and $\alpha = 0.5$ (panel a); $M = 0.5$, $K = 3.3$, $\lambda_1 = 0.7$, $\chi = 0.3$, $K_n = 0.15$, $R = 5$, and $\alpha = 0.5$ (panel b); $M = 1.5$, $K = 3.3$, $\lambda_1 = 0.7$, $\chi = 0.3$, $K_n = 0.15$, $R = 5$, and $\alpha = 0.5$ (panel c); $M = 0.01$, $K = 3.3$, $\lambda_1 = 1.2$, $\lambda_2 = 0.5$, $K_n = 0.15$, $R = 10$, and $\alpha = 0.5$ (panel d); $M = 0.01$, $K = 3.3$, $\lambda_1 = 0.7$, $\lambda_2 = 0.4$, $\chi = 0.1$, $R = 10$, and $\alpha = 0.5$ (panel e); $M = 0.01$, $K = 3.3$, $\lambda_1 = 0.7$, $\lambda_2 = 0.4$, $\chi = 0.6$, $R = 10$, and $\alpha = 0.5$ (panel f); $M = 0.01$, $K = 3.3$, $\lambda_1 = 0.7$, $\lambda_2 = 0.4$, $\chi = 0.9$, $R = 10$, and $\alpha = 0.5$ (panel g).

Fig. 5(a)–(g) display the variations of the mean velocity distribution and reversal flow with y for different values of λ_2, χ, and K_n. Fig. 5(a), (b), and (c) study the combined effect of λ_2 and M on the mean velocity distribution and reversal flow. It is revealed that at $M < 0.5$, the reversal flow decreases as the retardation time λ_2 gradually grows, afterwards, the effect of λ_2 almost vanishes for the critical value of $M(=0.5)$ (Fig. 5(b)). And finally, at $M > 0.5$, it is observed that λ_2 results in a slight increase in the reversal flow. This implies that the flow becomes slow with the increase of λ_2 due to the suppression effect of the retardation time. It is

Please cite this article in press as: S.I. Abdelsalam, K. Vafai, Combined effects of magnetic field and rheological properties on the peristaltic flow of a compressible fluid in a microfluidic channel, European Journal of Mechanics B/Fluids (2017), http://dx.doi.org/10.1016/j.euromechflu.2017.02.002

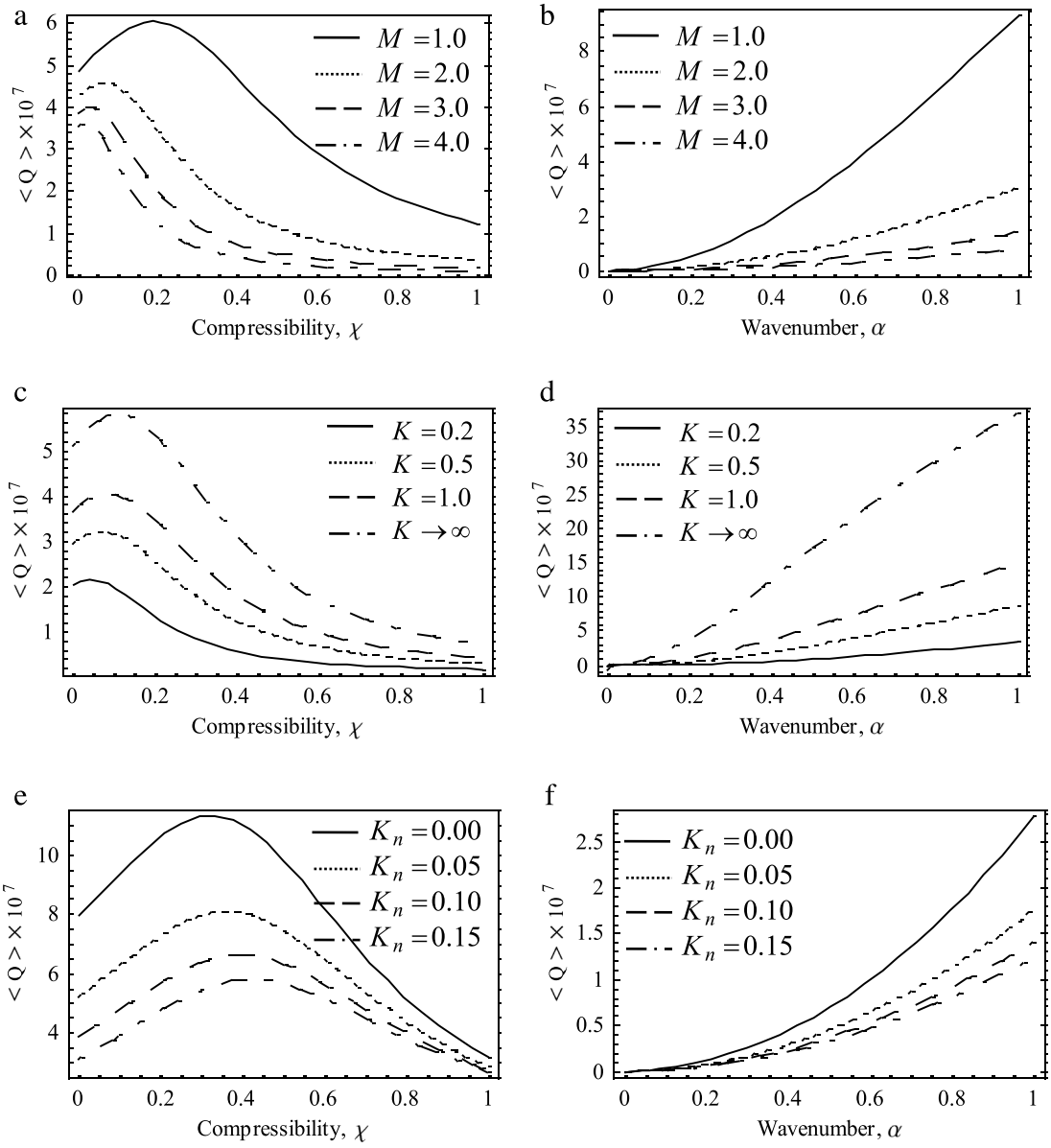

Fig. 6. The dimensionless net flow rate $\langle Q \rangle$ for: $K = 3.3$, $\lambda_1 = 1000$, $\lambda_2 = 200$, $K_n = 0.1$, $R = 100$, $\varepsilon = 0.001$, and $\alpha = 0.5$ (panel a); $K = 3.3$, $\lambda_1 = 1000$, $\lambda_2 = 200$, $K_n = 0.1$, $R = 100$, $\varepsilon = 0.001$, and $\chi = 0.6$ (panel b); $M = 1.5$, $\lambda_1 = 1000$, $\lambda_2 = 200$, $K_n = 0.1$, $R = 100$, $\varepsilon = 0.001$, and $\alpha = 0.5$ (panel c); $M = 0.4$, $\lambda_1 = 1000$, $\lambda_2 = 200$, $K_n = 0.15$, $R = 10$, $\varepsilon = 0.001$, and $\chi = 0.6$ (panel d); $M = 0.5$, $\lambda_1 = 1000$, $\lambda_2 = 400$, $K = 3.3$, $R = 100$, $\varepsilon = 0.001$, and $\alpha = 0.5$ (panel e); $M = 3$, $\lambda_1 = 1000$, $\lambda_2 = 200$, $K = 3.3$, $R = 100$, $\varepsilon = 0.001$, and $\chi = 0.6$ (panel f).

further noticed that the backflow of the Maxwell fluid is more than that of the Jeffrey's and which is a general observation that the velocity decreases with an increase in the viscoelastic parameter for viscoelastic fluids.

Fig. 5(d)–(g) describe the behavior of mean flow with χ and K_n. It is observed in Fig. 5(d) that the reversal flow decreases with an increase in χ. Fig. 5(e) through (g) show the combined effect of χ and K_n on the mean velocity distribution and reversal flow. It is clear that initially at $\chi < 0.6$, there will be reflux flow and a backward flow in the neighborhood of the center line occurring, and the mean axial velocity increases the reversal flow with increasing Knudsen number K_n; thus, the slip dependency prevails. This effect is then counterbalanced for $\chi = 0.6$, as shown in Fig. 5(f). Eventually, they are suppressed by the compressibility effect that dominates the flow and thus the mean axial velocity increases with increasing K_n and there is no reflux flow as shown in Fig. 5(g). It is further noticed that the mean velocity distribution has less magnitude for the nonslip fluid when compared to the slip fluid.

Fig. 6(a)–(f) show the variations of the net flow rate $\langle Q \rangle$ with χ and α for various values of M, K, and K_n. Several runs are made to our code for different values of these parameters in order to validate the results. We investigate the effect of M on $\langle Q \rangle$, and we notice that M has a decreasing effect on $\langle Q \rangle$ at any value for χ and α as shown in Fig. 6(a) and (b). It may be physically interpreted that the fluid requires a better pump to maintain the same flow rate under an increased magnetic field. In Fig. 6(a), we investigate the dependence of $\langle Q \rangle$ on χ for various values of M. We notice that for $M = 1$, the net flow rate $\langle Q \rangle$ reaches its maximum at $\chi = 0.22$. Further, for $M = 2$, the maximum value of $\langle Q \rangle$ occurs at $\chi = 0.1$. Moreover, for $M = 4$ and $M = 6$, we notice that the maximum value of $\langle Q \rangle$ occurs at $\chi = 0.05$ and $\chi = 0.04$, respectively. So that we have a similar fashion that suggests that there is a critical value for M at which the flow reaches its maximum before it decays. This endorses the findings given above.

In Fig. 6(c) and (d), we investigate the dependence of $\langle Q \rangle$ on the compressibility parameter χ and on the wave number α for

Please cite this article in press as: S.I. Abdelsalam, K. Vafai, Combined effects of magnetic field and rheological properties on the peristaltic flow of a compressible fluid in a microfluidic channel, European Journal of Mechanics B/Fluids (2017), http://dx.doi.org/10.1016/j.euromechflu.2017.02.002

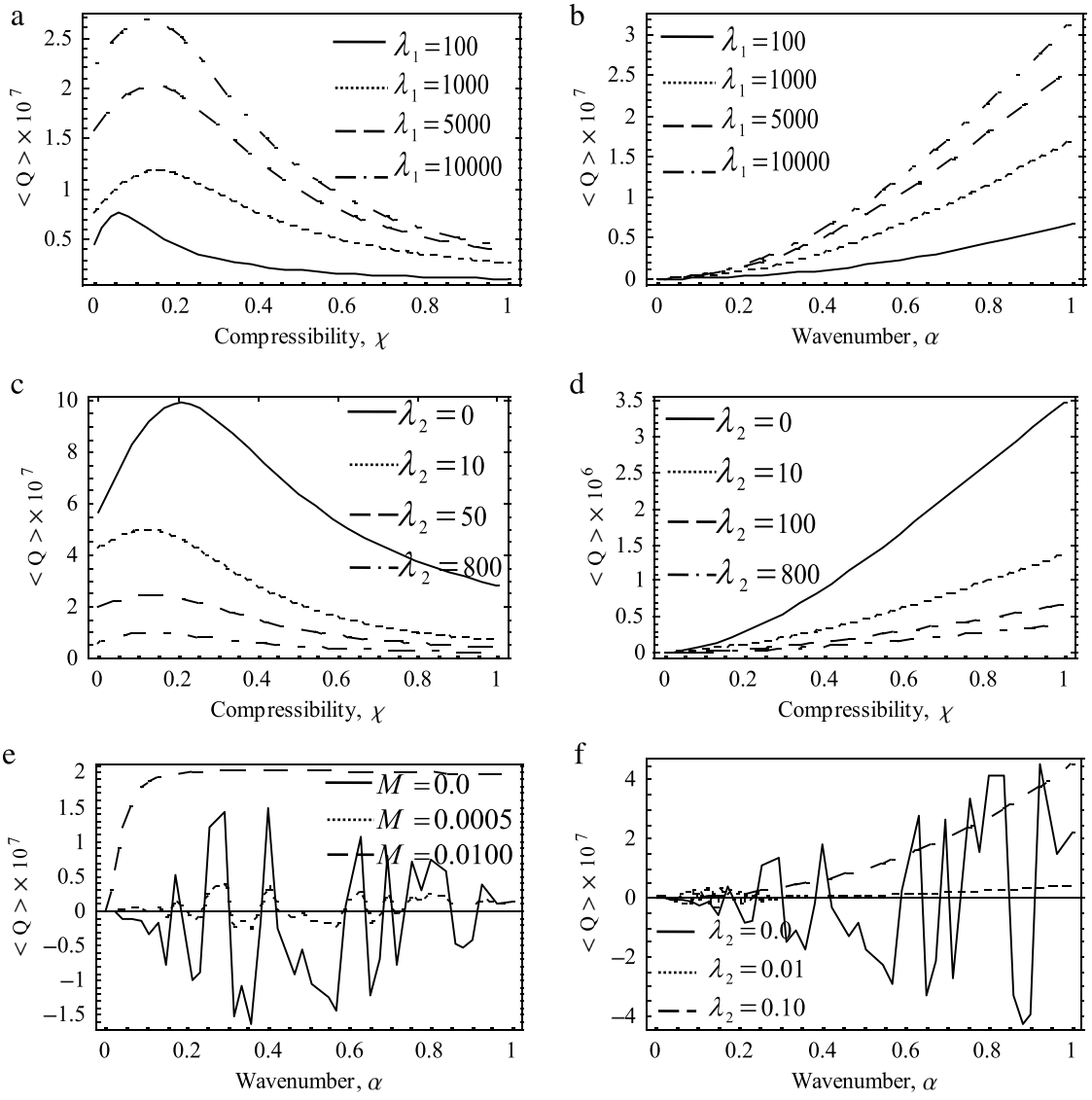

Fig. 7. The dimensionless net flow rate $\langle Q \rangle$ for: $M = 1.5$, $\lambda_2 = 400$, $K_n = 0.05$, $K = 1$, $R = 10\,000$, $\varepsilon = 0.001$, and $\alpha = 0.5$ (panel a); $M = 1.5$, $\lambda_2 = 400$, $K_n = 0.05$, $K = 1$, $R = 10\,000$, $\varepsilon = 0.001$, and $\chi = 0.6$ (panel b); $M = 1.5$, $\lambda_1 = 1000$, $K_n = 0.05$, $K = 1$, $R = 10\,000$, $\varepsilon = 0.001$, and $\alpha = 0.5$ (panel c); $M = 1$, $\lambda_1 = 1000$, $K_n = 0.05$, $K = 3.3$, $R = 10\,000$, $\varepsilon = 0.001$, and $\chi = 0.6$ (panel d); $\lambda_1 = 1000$, $\lambda_2 = 0.001$, $K_n = 0.15$, $K = 3.3$, $R = 10\,000$, $\varepsilon = 0.001$, and $\chi = 0.6$ (panel e); $\lambda_1 = 1000$, $M = 0.0001$, $K_n = 0.15$, $K = 3.3$, $R = 10\,000$, $\varepsilon = 0.001$, and $\chi = 0.6$ (panel f).

various values of K. We observe that the flow rate increases with increasing K at any value for χ and α. In Fig. 6(c), we notice that $\langle Q \rangle$ reaches its maximum value at a small value of χ (=0.1) for all values of K before decay. The results are quite opposite to those obtained in [4] for the MHD Maxwell fluid where $\langle Q \rangle$ attains its maximum at $\chi = 0.9$. One possible reason is that the flow becomes slow with the existence of λ_2 due to the suppression effect of the retardation time. Fig. 6(e) and (f) are plotted so as to investigate the dependence of $\langle Q \rangle$ on χ and α for various values of the slip parameter K_n. We set K_n to different values and investigate the changes induced by it. We observe that $\langle Q \rangle$ decreases by increasing K_n at any value of χ or α. Moreover, we notice in Fig. 6(e). that the maximum value for $\langle Q \rangle$ occurs at $\chi = 0.35$ for all values of K_n. It is also shown that the flow rate has more magnitude for the nonslip fluid when compared with the slip fluid.

Fig. 7(a)–(f) show the variations of the net flow rate $\langle Q \rangle$ with χ and α for various values of λ_1, λ_2, and M. In order to investigate the dependence of the flow rate $\langle Q \rangle$ on λ_1, we perform the calculations for few values of λ_1 in Fig. 7(a) and (b). We notice that $\langle Q \rangle$ increases with increasing λ_1 at any value of χ and α. It is noticed in Fig. 7(a) that $\langle Q \rangle$ reaches its maximum value at $\chi = 0.07$ for $\lambda_1 = 100$, while it reaches its maximum at relatively higher value of χ(=0.15) for $\lambda_1 \geq 1000$. The latter result justifies the strong viscoelastic effect discussed in [8,35] for $\lambda_1 > 859.11$. We are going to shed some light on this later on. Moreover, the most significant difference between the peaks of λ_1 given in Fig. 7(a) and those given in Fig. 4(g) of [4] is that the introduction of λ_2 into the MHD flow results in shifting the maximum of flow rate towards lower values χ rather than higher values. Nevertheless, we observe in Fig. 7(b) the absence of maximum and the rapid growth of $\langle Q \rangle$ in the considered interval of variation of α.

A code has been written to calculate $\langle Q \rangle$ in order to investigate its dependence upon λ_2 for χ and α as given in Fig. 7(c) and (d). We notice that $\langle Q \rangle$ decreases with increasing λ_2 at any value of χ and α. It is noticed in Fig. 7(c) that there is a plateau initially corresponds to essentially Maxwellian fluid flow where its maximum is higher than those of the Jeffrey's. To wit, $\langle Q \rangle$ reaches its maximum value at $\chi = 0.2$ for the Maxwell's fluid model (solid line), while it decays rapidly and reaches its maximum at a lower value of χ for the Jeffrey fluid model. Also, the peaks of $\langle Q \rangle$ for the Jeffrey fluid take place at an identical point of χ (=0.125). Fig. 7(c) shows that for $\lambda_2 = 10$, there is a slight deviation from the

Please cite this article in press as: S.I. Abdelsalam, K. Vafai, Combined effects of magnetic field and rheological properties on the peristaltic flow of a compressible fluid in a microfluidic channel, European Journal of Mechanics B/Fluids (2017), http://dx.doi.org/10.1016/j.euromechflu.2017.02.002

Maxwellian limiting case (solid line), which translates into shifting the maximum towards smaller values of χ. For $\lambda_2 = 100$ and $\lambda_2 = 800$, we notice further deviation from the Maxwellian flow, which also translates into shifting the maximum towards smaller values of χ. We notice, in Fig. 7(d), a much drastic change which is the absence of maximum and the rapid decay of $\langle Q \rangle$ in the considered interval of variation of α. This pattern conforms to the results obtained by [8], since large λ_1 (>859.11 measured in units of d/c) means that the system exhibits strong viscoelastic behavior as suggested by [8,35]. And since we have chosen that $\lambda_2 < \lambda_1$ as suggested in [29], therefore the swift decrease in the curves for various values of λ_2 at the same value of λ_1(=1000) is justified. Additional detailed analytical and operational characteristics of fluidic cells and microchannels can be found in Refs. [36–40].

In order to investigate further combined effects of the retardation time and magnetic parameter on $\langle Q \rangle$ for various values of χ and α, we fixed both of $\lambda_2 = 0.001$ and $M = 0.0001$ in Fig. 7(e) and (f), successively. We investigate novelties brought about by the introduction of the λ_2 and M into the model. We treat these cases individually due to the appearance of the negative flow rates for certain values of α which implies to the existence of flow in the reverse direction to the direction of propagation of traveling wave on the wall of the microchannel. In Fig. 7(e), it is shown that for $\alpha \geq 0.05$, $\langle Q \rangle$ becomes negative at $\lambda_2 = 0.001$ and $\lambda_1 = 1000$ and we observe a backflow for various values of M. It is noticed that the behavior of $\langle Q \rangle$ for our Jeffrey model in the absence of M (the solid line with numerous maxima) is highly oscillatory just like what was observed for the Maxwell model in [4]. The possible reasons for this striking nonlinear response of this complex biological material are: 1. the aforementioned strong viscoelastic behavior of the viscoelastic parameters, 2. the large Reynolds number that leads to quick oscillations of the flow profiles with smaller amplitudes [1]. The latter result agrees qualitatively with that obtained in [30]. In addition, it is observed that these oscillations decay rapidly with increasing M and the effect of retardation time becomes weak. The possible reason is that the opposing magnetic force play a significant role and exceeds the elastic force. It is thus concluded that increasing the magnetic parameter makes the fluid less prone to nonlinear effects.

Finally, we investigate the disturbances caused by the deeply non-Newtonian regime in the presence of magnetic field in Fig. 7(f). It is noticed that at $M = 0.0001$, the Maxwell fluid (the solid line) is highly oscillatory. The resultant nonlinear stress from the deformation is not new, however, the quick decay of the oscillations of the MHD flow with increasing the retardation time for a compressible fluid is unusual. This implies to an obvious suppression effect of λ_2 to the flow rate of Jeffrey fluid. And thus, the oscillation decay is highly dependent upon λ_2 which occurs in the constitutive equation of the Jeffrey fluid.

It is further proposed that the possibility of flow in the direction opposite to the propagation of the traveling wave on the channel wall does not only exist due to rheological behavior (which is characterized using an oscillatory deformation protocol), but also due to the effect of acoustic streaming. This is due to the fact that the acoustic wave propagating in the conduit induces a mean flow in the opposite direction in the central part of the conduit [8]. The mean flow of acoustic streaming is caused by the presence of friction at the bounding surfaces of the channel. This effect is rather quadratic than linear. Little explored thus far in microfluidics, the inertial nonlinearity can rectify oscillatory fluid motion to give the acoustic streaming flow [41].

Special cases: Comparing with other models for verifications of results, the present model gives a general form of fluid flow analysis from which other mathematical models can be easily derived by proper substitutions. In some cases, our results reduce to those for Maxwell and Newtonian fluids. Some of which:

1. Adjusting $\lambda_2 = 0$ in our investigation implies to the results of MHD compressible Maxwell fluid obtained by Mekheimer et al. [4].
2. Choosing $\chi = 0$, $K_n = 0$, and $K \to \infty$ in our investigation implies to a well-agreed physical situation for MHD Jeffrey fluid flow through a microchannel in the absence of electric field as obtained by Si and Jian [1].
3. The results of the compressible Jeffrey fluid filling the non-porous 2D microchannel with noncompliant walls of Hayat et al. [23] can be obtained by taking $M = 0$, and $K \to \infty$ in our analysis.
4. Setting $M = 0$, $K_n = 0$, and $K \to \infty$ in our study leads to the results for the compressible non-Newtonian fluid in a tube of Hayat et al. [30].
5. The rheological effects on MHD peristaltic flow of incompressible Jeffrey fluid with noncompliant walls of Hayat et al. [24] can be restored by setting $\chi = 0$, $K_n = 0$, and $K \to \infty$ in our investigation.
6. Our results agrees with the results of Eldesoky and Mousa [20] when taking $M = 0$, $K_n = 0$, and $\lambda_2 = 0$ in our study.
7. The results of compressible viscous fluid filling the non-porous medium with noncompliant walls of Mekheimer and Abdel-Wahab [14] can be recovered by setting $M = 0$, $\lambda_1 = 0$, $\lambda_2 = 0$, and $K \to \infty$ in our research.
8. Setting $\lambda_2 = 0$, $M = 0$, $K_n = 0$, and $K \to \infty$ implies to the outcomes of the analysis for compressible fluids that were given by Tsiklauri and Beresnev [8].

5. Conclusions

In this study, we have obtained the analytical solution of MHD peristaltic flow of a compressible Jeffrey fluid induced by a surface acoustic wave though microparallel plates having slip at the walls. The medium is considered porous and the problem is discussed for the free pumping case. We discuss the impact of combined effects of magnetic field and viscoelastic parameters on the flow. The main findings can be summarized as follows:

(i) There are critical values of M for the mean velocity at the boundaries and perturbation function around which the increasing effect of relaxation time on the functions has an opposite trend.
(ii) Critical values of M are found after which the decreasing effect of retardation time on the perturbation function and reversal flow is reversed.
(iii) There is a critical value found for M that causes the increasing influence of compressibility parameter on the perturbation function to be reversed.
(iv) There is an optimum value of M at which the net flow rate is maximum.
(v) Increasing the magnetic parameter makes the fluid less prone to nonlinear effects.
(vi) High values of magnetic field and Reynolds number cause the perturbed velocity to be flattened around the centerline of the microfluidic channel maintaining the mirror of symmetry.
(vii) The combined effect of the slip parameter and the compressibility causes the slip parameter to initially dominate both the mean velocity distribution and the perturbation function, but by increasing the compressibility parameter, the effect is counterbalanced and then suppressed leaving no reflux flow.
(viii) The flow becomes slow with the existence of the retardation time due to the suppression effect.
(ix) The introduction of the retardation time into the MHD flow results in shifting the maximum of flow rate towards lower values χ rather than higher values.

Please cite this article in press as: S.I. Abdelsalam, K. Vafai, Combined effects of magnetic field and rheological properties on the peristaltic flow of a compressible fluid in a microfluidic channel, European Journal of Mechanics B/Fluids (2017), http://dx.doi.org/10.1016/j.euromechflu.2017.02.002

(x) Unlike the flow rate, the perturbation function and the mean velocity distribution has less magnitude for the nonslip flow when compared to the slip flow.
(xi) Oscillations decay rapidly with increasing the magnetic parameter, and the effect of retardation time becomes weak.
(xii) The quadratic effect of acoustic streaming causes the possibility of flow to be in an opposite direction to the propagation of traveling wave.

Acknowledgments

Sara I. Abdelsalam thanks the Binational Fulbright Commission in Egypt and the Council for International Exchange of Scholars in the USA for the honor of the Fulbright Egyptian Scholar Award for the year 2015–2016. Sara I. Abdelsalam is also grateful for Professor John Brady, Division of Chemistry and and Chemical Engineering in Caltech, for his support.

Appendix

The variables and parameters obtained in Section 3 for the first-order solution are given by:

$$\gamma = \gamma^* R - \frac{i\alpha\chi}{3}, \qquad \beta_1^2 = \alpha^2 - i\alpha\gamma^* R + \frac{R}{K},$$

$$a_1^2 = \frac{(\beta^2+\upsilon^2) + \sqrt{(\beta^2+\upsilon^2)^2 - 4\beta_1^2\upsilon_1^2}}{2},$$

$$a_2^2 = \frac{(\beta^2+\upsilon^2) - \sqrt{(\beta^2+\upsilon^2)^2 - 4\beta_1^2\upsilon_1^2}}{2},$$

$$b_1 = \chi\frac{(a_1^2-\beta_1^2)}{\gamma a_1} + \frac{i a_1}{\alpha}, \qquad b_2 = \chi\frac{(a_2^2-\beta_1^2)}{\gamma a_2} + \frac{i a_2}{\alpha},$$

$$C_1 = \frac{i\alpha}{2}\frac{b_2 g_2}{G}, \qquad C_2 = -\frac{i\alpha}{2}\frac{1}{\sinh a_2}\left(1 + \frac{\sinh a_1}{G} b_2 g_2\right),$$

and $C_3 = 0$

such that $\beta^2 = \alpha^2 - i\alpha\gamma^* R + \frac{R}{K} + M R\gamma^*$, $G = b_1 g_1 \sinh a_2 - b_2 g_2 \sinh a_1, \upsilon^2 = \beta_1^2 - \frac{\left(\beta_1^2-\alpha^2\right)}{\Gamma}$, and $\upsilon_1^2 = \beta^2 - \frac{(\beta^2-\alpha^2)}{\Gamma}$, with $g_1 = \cosh a_1 + K_n a_1 \sinh a_1, g_2 = \cosh a_2 + K_n a_2 \sinh a_2$, and $\Gamma = 1 - \frac{i\alpha\chi}{\gamma}$.

The expressions of υ and υ_1 can be written in terms of $\gamma^*, R, \alpha, K, M$ and χ as

$$\upsilon^2 = \frac{-\frac{i4}{3}\alpha^3\chi + \alpha^2\gamma^* R(1-\chi) - \frac{i\alpha\chi R}{K}}{R\gamma^* - \frac{i4\alpha\chi}{3}},$$

$$\upsilon_1^2 = \frac{-\frac{i4}{3}\alpha^3\chi + \alpha^2\gamma^* R(1-\chi) - i\alpha\chi R\left(M\gamma^* + \frac{1}{K}\right)}{R\gamma^* - \frac{i4\alpha\chi}{3}}.$$

Notice that $\gamma^* = \gamma_1$ for $\lambda_2 = 0$ which conforms to the results obtained by Mekheimer et al. [4] for the Maxwell fluid model.

For the second-order solutions, the complex constants follow from the boundary conditions and are given by:

$$D_1 = \frac{i\alpha}{2} K_n\left(\overline{U_1'}(1) - U_{1,(1)}'\right),$$

$$D_4 = P_{20}(-1) + 4\chi H(-1)/3R,$$

$$D_2 = \frac{-1}{2(\cosh\delta + K_n\delta\sinh\delta)} \times \left[K_n\left(E'(1) - E'(-1)\right) + K_n(\beta_4 - \beta_5) + \beta_2 + \beta_3 + E(1) + E(-1)\right],$$

$$D_3 = \frac{-1}{2(\sinh\delta + K_n\delta\cosh\delta)} \times \left[K_n\left(E'(1) + E'(-1)\right) + K_n(\beta_4 + \beta_5) + \beta_2 - \beta_3 + E(1) - E(-1)\right],$$

such that the function F and H are given by

$$F = i\alpha\chi P_1\overline{V_1} - i\alpha\overline{P_1}V_1 + V_1\overline{V_1'} + V_1'\overline{V_1} - i\alpha U_1\overline{V_1} + i\alpha\overline{U}_1 V_1, \qquad H = \frac{d}{dy}\left(P_1\overline{V_1} + \overline{P}_1 V_1\right),$$

where

$$\beta_2 = \frac{1}{2}\left(U_1'(1) + \overline{U_1'}(1)\right), \qquad \beta_3 = -\frac{1}{2}\left(U_1'(-1) + \overline{U_1'}(-1)\right),$$

$$\beta_4 = \frac{1}{2}\left(U_1''(1) + \overline{U_1''}(1)\right), \qquad \beta_5 = -\frac{1}{2}\left(U_1''(-1) + \overline{U_1''}(-1)\right),$$

$$\begin{aligned} E(y) = R\Bigg\{ & \frac{j_1}{(a_1+\overline{a_1})^2-\delta^2}\cosh(a_1+\overline{a_1})y + \frac{j_{11}}{(a_1-\overline{a_1})^2-\delta^2}\cosh(a_1-\overline{a_1})y \\ & + \frac{j_2}{(a_1+\overline{a_2})^2-\delta^2}\cosh(a_1+\overline{a_2})y + \frac{j_{22}}{(a_1-\overline{a_2})^2-\delta^2}\cosh(a_1-\overline{a_2})y \\ & + \frac{j_3}{(a_2+\overline{a_1})^2-\delta^2}\cosh(a_2+\overline{a_1})y + \frac{j_{33}}{(a_2-\overline{a_1})^2-\delta^2}\cosh(a_2-\overline{a_1})y \\ & + \frac{j_4}{(a_2+\overline{a_2})^2-\delta^2}\cosh(a_2+\overline{a_2})y + \frac{j_{44}}{(a_2-\overline{a_2})^2-\delta^2}\cosh(a_2-\overline{a_2})y\Bigg\}, \end{aligned}$$

$$\begin{aligned} j_1 = {} & \frac{1}{2}(a_1 C_1\overline{b_1}\,\overline{C_1} + \overline{a_1}\,\overline{C_1} b_1 C_1 + \overline{a_1}\,\overline{b_1}\,\overline{C_1} C_1 + a_1 b_1 C_1\overline{C_1}), \\ j_2 = {} & \frac{1}{2}(a_1 C_1\overline{b_2}\,\overline{C_2} + \overline{a_2}\,\overline{C_2} b_1 C_1 + \overline{a_2}\,\overline{b_2}\,\overline{C_2} C_1 + a_1 b_1 C_1\overline{C_2}), \\ j_3 = {} & \frac{1}{2}(a_2 C_2\overline{b_1}\,\overline{C_1} + \overline{a_1}\,\overline{C_1} b_2 C_2 + \overline{a_1}\,\overline{b_1}\,\overline{C_1} C_2 + a_2 b_2 C_2\overline{C_1}), \\ j_4 = {} & \frac{1}{2}(a_2 C_2\overline{b_2}\,\overline{C_2} + \overline{a_2}\,\overline{C_2} b_2 C_2 + \overline{a_2}\,\overline{b_2}\,\overline{C_2} C_2 + a_2 b_2 C_2\overline{C_2}), \\ j_{11} = {} & \frac{1}{2}(a_1 C_1\overline{b_1}\,\overline{C_1} + \overline{a_1}\,\overline{C_1} b_1 C_1 - \overline{a_1}\,\overline{b_1}\,\overline{C_1} C_1 - a_1 b_1 C_1\overline{C_1}), \\ j_{22} = {} & \frac{1}{2}(a_1 C_1\overline{b_2}\,\overline{C_2} + \overline{a_2}\,\overline{C_2} b_1 C_1 - \overline{a_2}\,\overline{b_2}\,\overline{C_2} C_1 - a_1 b_1 C_1\overline{C_2}), \\ j_{33} = {} & \frac{1}{2}(a_2 C_2\overline{b_1}\,\overline{C_1} + \overline{a_1}\,\overline{C_1} b_2 C_2 - \overline{a_1}\,\overline{b_1}\,\overline{C_1} C_2 - a_2 b_2 C_2\overline{C_1}), \\ j_{44} = {} & \frac{1}{2}(a_2 C_2\overline{b_2}\,\overline{C_2} + \overline{a_2}\,\overline{C_2} b_2 C_2 - \overline{a_2}\,\overline{b_2}\,\overline{C_2} C_2 - a_2 b_2 C_2\overline{C_2}). \end{aligned}$$

References

[1] D. Si, Y. Jain, Electromagnetohydrodynamic (EMHD) micropump of Jeffrey fluids through two parallel microchannels with corrugated walls, J. Phys. D: Appl. Phys. 48 (2015) 085501. [10 pages].
[2] H. Kabbani, A. Wang, X. Luo, S. Qian, Modeling RedOx-based magnetohydrodynamics in three-dimensional microfluidic channels, Phys. Fluids 19 (2007) 083604. [1–12].

Please cite this article in press as: S.I. Abdelsalam, K. Vafai, Combined effects of magnetic field and rheological properties on the peristaltic flow of a compressible fluid in a microfluidic channel, European Journal of Mechanics B/Fluids (2017), http://dx.doi.org/10.1016/j.euromechflu.2017.02.002

[3] D.Y. Lee, K. Vafai, Comparative analysis of jet impingement and microchannel cooling for high heat flux applications, Int. J. Heat Mass Transfer 42 (1999) 1555–1568.
[4] Kh.S. Mekheimer, S.R. Komy, S.I. Abdelsalam, Simultaneous effects of magnetic field and space porosity on compressible Maxwell fluid transport induced by a surface acoustic wave in a microchannel, Chin. Phys. B 22 (2013) 124702. [10 pages].
[5] Kh.S. Mekheimer, A.N. Abdel-Wahab, Net annulus flow of a compressible viscous liquid with peristalsis, J. Aerosp. Eng. 25 (2012) 660–669.
[6] K. Vafai, A.-R.A. Khaled, Analysis of flexible microchannel heat sink systems, Int. J. Heat Mass Transfer 48 (2005) 1739–1746.
[7] A.R.A. Khaled, K. Vafai, Cooling augmentation using microchannels with rotatable separating plates, Int. J. Heat Mass Transfer 54 (2011) 3732–3739.
[8] D. Tsiklauri, I. Beresnev, Non-Newtonian effects in the peristaltic flow of a Maxwell fluid, Phys. Rev. E 64 (2001) 03630. [5 pages].
[9] A.C.T. Aarts, G. Ooms, Net flow of compressible viscous liquids induced by travelling waves in porous media, J. Eng. Math. 34 (1998) 435–450.
[10] Q. Qi, R.E. Johnson, J.G. Harris, Boundary layer attenuation and acoustic streaming accompanying plane-wave propagation in a tube, J. Acoust. Soc. Am. 97 (1995) 1499–1509.
[11] F.W. Beil, A. Wixforth, R.H. Blick, Investigation of nano-electromechanical-systems using surface acoustic waves, Physica E 13 (2002) 473–476.
[12] W.-I. Chen, Influence of ultrasonic energy upon the rate of flow of liquids through porous media (Ph.D. thesis), West Virginia Univ., Morgantown, WV, 1969.
[13] K.-H.W. Chu, Transport within a microtube induced by a surface acoustic wave, Eur. Phys. J. Appl. 13 (2001) 147–152.
[14] Kh.S. Mekheimer, A.N. Abdel-Wahab, Effect of wall compliance on compressible fluid transport induced by a surface acoustic wave in a Microchannel, Inc. Numer. Methods Partial Differ. Equ. 27 (2011) 621–636.
[15] S.A. Schaaf, P.L. Chambre, Flow of Rarefied Gases, Princeton University Press, Princeton, 1961.
[16] B.K. Jha, B. Aina, A.T. Ajiya, MHD natural convection flow in a vertical parallel plate microchannel, Ain Shams Eng. J. 6 (2015) 289–295.
[17] E.F. El-Shehawy, N.T. El-Dabe, I.M. El-Desoky, Slip effects on the peristaltic flow of a non-Newtonian Maxwellian fluid, J. Acta Mech. 186 (2006) 141–159.
[18] W. Kwang-Hua Chu, J. Fang, Peristaltic transport in a slip flow, Eur. Phys. J. B 16 (2000) 543–547.
[19] Y.C. Fung, C.S. Yih, Peristaltic transport, J. Appl. Mech. 35 (1968) 669–675.
[20] I.M. Eldesoky, A.M. Abdallah, Peristaltic Pumping of Fluid in Cylindrical Tube and its Applications in the Field of Aerospace, ASAT-13-FL-01, 2009, pp. 1–14.
[21] Y. Abd Elmaboud, Kh.S. Mekheimer, S.I. Abdelsalam, A study of nonlinear variable viscosity in finite-length tube with peristalsis, Appl. Bionics Biomech. 11 (2014) 197–206.
[22] K. Vafai, A.A. Khan, S. Sajjad, R. Ellahi, The study of peristaltic motion of third grade fluid under the effects of Hall current and heat transfer, Z. Naturforsch. 70 (2015) 281–293.
[23] T. Hayat, M. Javed, A.A. Hendi, Wall compliance effect on the flow of compressible non-Newtonian fluid, J. Mech. Med. Biol. 12 (2012) 125004. [14 pages].
[24] T. Hayat, M. Javed, S. Asghar, S. Mesloub, Compliant wall analysis of an electrically conducting Jeffrey fluid with peristalsis, Z. Naturforsch. 66a (2011) 106–116.
[25] R.H. Ewoldt, A.E. Hosoi, G.H. McKinley, Nonlinear viscoelastic biomaterials: Meaningful characterization and engineering inspiration, Integr. Comp. Biol. 49 (1) (2009) 40–50.
[26] A.A. Khan, R. Ellahi, K. Vafai, Peristaltic transport of a Jeffrey fluid with variable viscosity through a porous medium in an asymmetric channel, Adv. Math. Phys. 2012 (2012) 169642. [15 pages].
[27] M. Lasiello, K. Vafai, A. Andreozzi, N. Bianco, F. Tavakkoli, Effects of external and internal hyperthermia on LDL transport and accumulation within an arterial wall in the presence of stenosis, Ann. Biomed. Eng. 43 (2014) 1585–1599.
[28] K. Wang, F. Tavakkoli, S. Wang, K. Vafai, Analysis and analytical characterization of bioheat transfer during radiofrequency ablation, J. Biomech. 48 (2015) 930–940.
[29] C. Gao, Y. Jian, Analytical solution of magnetohydrodynamic flow of Jeffrey fluid through a circular microchannel, J. Mol. Liq. 211 (2015) 803–811.
[30] T. Hayat, N. Ali, S. Asghar, An analysis of peristaltic transport for flow of a Jeffrey fluid, Acta Mech. 193 (2007) 101–112.
[31] S.R. El koumy, E.S.B. Barakat, S.I. Abdelsalam, Hall and porous boundaries effects on peristaltic transport through porous medium of a Maxwell model, Transp. Porous Media 94 (2012) 643–658.
[32] S.R. Elkoumy, E.I. Barakat, S.I. Abdelsalam, Hall and transverse magnetic field effects on peristaltic flow of a Maxwell fluid through a porous medium, Global J. Pure Appl. Math. 9 (2) (2013) 187–203.
[33] Y. Damianou, G.C. Georgiou, I. Moulitsas, Combined effects of compressibility and slip in flows of a Herschel-Bulkley fluid, J. Non-Newton. Fluid Mech. 193 (2013) 89–102.
[34] W.C. Tan, T. Masuoka, Stokes' first problem for an Oldroyd-B fluid in a porous half space, Phys. Fluids 17 (2005) 023107.
[35] J.A. del Rio, M.L. de Haro, S. Whitaker, Enhancement in the dynamic response of a viscoelastic fluid flowing in a tube, Phys. Rev. E 58 (1998) 124702–6327.
[36] A.R.A. Khaled, K. Vafai, Analysis of oscillatory flow disturbances and thermal characteristics inside fluidic cells due to fluid leakage and wall slip conditions, J. Biomech. 37 (2004) 721–729.
[37] K. Khanafer, K. Vafai, Geometrical and flow configurations for enhanced microcantilever detection within a fluidic cell, Int. J. Heat Mass Transfer 48 (2005) 2886–2895.
[38] A.R.A. Khaled, K. Vafai, Analysis of thermally expandable flexible fluidic thin film channels, ASME J. Heat Transfer 129 (2007) 813–818.
[39] S. Mahjoob, K. Vafai, N.R. Beer, Rapid microfluidic thermal cycler for polymerase chain reaction nucleic acid amplification, Int. J. Heat Mass Transfer 51 (2008) 2109–2122.
[40] K. Vafai, L. Zhu, Analysis of a two-layered micro-channel heat sink concept in electronic cooling, Int. J. Heat Mass Transfer 42 (1999) 2287–2297.
[41] T.M. Squires, S.R. Quake, Microfluidics: Fluid physics at the nanoliter scale, Rev. Modern Phys. 77 (2005) 977–1026.

Please cite this article in press as: S.I. Abdelsalam, K. Vafai, Combined effects of magnetic field and rheological properties on the peristaltic flow of a compressible fluid in a microfluidic channel, European Journal of Mechanics B/Fluids (2017), http://dx.doi.org/10.1016/j.euromechflu.2017.02.002